# Redox-Regulation of Photorespiration through Mitochondrial Thioredoxin o1[1]

**Ole Reinholdt,[a,2] Saskia Schwab,[a] Youjun Zhang,[b,c] Jean-Philippe Reichheld,[d,e] Alisdair R. Fernie,[b,c] Martin Hagemann,[a] and Stefan Timm[a,3,4]**

[a]University of Rostock, Plant Physiology Department, Albert-Einstein-Straße 3, D-18059 Rostock, Germany
[b]Max Planck Institute of Molecular Plant Physiology, Am Mühlenberg 1, D-14476 Golm, Germany
[c]Center of Plant System Biology and Biotechnology, 4000 Plovdiv, Bulgaria
[d]Laboratoire Génome et Développement des Plantes, CNRS, F-66860 Perpignan, France
[e]Laboratoire Génome et Développement des Plantes, Université Perpignan Via Domitia, F-66860 Perpignan, France

**ORCID IDs: 0000-0003-1052-0256 (Y.Z.); 0000-0001-9000-335X (A.R.F.); 0000-0002-2059-2061 (M.H.); 0000-0003-3105-6296 (S.T.).**

Photorespiration sustains photosynthesis in the presence of oxygen due to rapid metabolization of 2-phosphoglycolate, the major side-product of the oxygenase activity of Rubisco that also directly impedes carbon assimilation and allocation. Despite the fact that both the biochemical reactions and the underlying genetics are well characterized, information concerning the regulatory mechanisms that adjust photorespiratory flux is rare. Here, we studied the impact of mitochondrial-localized thioredoxin o1 (TRXo1) on photorespiratory metabolism. The characterization of an Arabidopsis (*Arabidopsis thaliana*) transfer DNA insertional line (*trxo1-1*) revealed an increase in the stoichiometry of photorespiratory $CO_2$ release and impaired Gly-to-Ser turnover after a shift from high-to-low $CO_2$ without changes in Gly decarboxylase (GDC) gene or protein expression. These effects were distinctly pronounced in a double mutant, where the *TRXo1* mutation was combined with strongly reduced GDC T-protein expression. The double mutant (*TxGT*) showed reduced growth in air but not in high $CO_2$, decreased photosynthesis, and up to 54-fold more Gly alongside several redox-stress-related metabolites. Given that GDC proteins are potential targets for redox-regulation, we also examined the in vitro properties of recombinant GDC L-proteins (lipoamide dehydrogenase) from plants and the cyanobacterium *Synechocystis species* strain PCC6803 and observed a redox-dependent inhibition by either artificial reducing agents or TRXo1 itself. Collectively, our results demonstrate that TRXo1 potentially adjusts photorespiration via redox-regulation of GDC in response to environmental changes.

Photorespiration is an essential process in all organisms performing oxygenic photosynthesis, because it is intrinsically linked to photosynthetic $CO_2$ fixation via Rubisco, which catalyzes carboxylation but also oxygenation (Bauwe et al., 2012; Appel et al., 2013). During carboxylation, $CO_2$ is incorporated into the acceptor, ribulose-1,5-bisphosphate, leading to the formation of two 3-phosphoglycerate (3-PGA) molecules that enter the Calvin-Benson cycle (CBC). In the Rubisco oxygenase reaction, ribulose-1,5-bisphosphate accept $O_2$, yielding one 3-PGA and one 2-phosphoglycolate (2-PG) molecule (Bowes et al., 1971). 2-PG is a non-CBC intermediate that is exclusively metabolized by the photorespiratory C2 cycle (Somerville and Ogren, 1979). In addition to the main function of photorespiration as an organic carbon salvage pathway, efficient 2-PG degradation is essential for plant metabolism, because 2-PG acts as a potent inhibitor of many enzymes in the chloroplastidial stroma, such as triose-phosphate isomerase, phosphofructokinase, and sedoheptulose-1,7-bisphosphate phosphatase (Anderson, 1971; Kelly and Latzko, 1976; Flügel et al., 2017; Levey et al., 2019; Li et al., 2019). Hence, 2-PG accumulation significantly reduces the efficiency of $CO_2$ assimilation through impairment of the CBC and starch biosynthesis.

Following the early discovery of light-induced photorespiratory gas-exchange (Zelitch, 1964; Ogren and Bowes, 1971; Tolbert, 1971), a broad range of photorespiratory

[1]This work was supported by the University of Rostock (to M.H. and S.T.). The LC-MS equipment at the University of Rostock was financed through the Hochschulbauförderungsgesetz program (GZ: INST 264/125-1 FUGG). This study is set within the framework of the Laboratoires d'Excellences (Labex) TULIP (ANR-10-LABX-41).

[2]Present address: Miltenyi Biotec GmbH, Robert-Koch-Straße 1, 17166 Teterow, Germany.

[3]Author for contact: stefan.timm@uni-rostock.de.

[4]Senior author.

The author responsible for distribution of materials integral to the findings presented in this article in accordance with the policy described in the Instructions for Authors (www.plantphysiol.org) is: Stefan Timm (Stefan.timm@uni-rostock.de).

O.R., S.S., Y.Z., and S.T. performed the research and analyzed data; J.-P.R. provided expression clones for TRXo1 and NTRa and A.R.F. the T-DNA insertional mutant *trxo1-1*; A.R.F. and M.H. provided experimental equipment and tools; S.T. wrote the article, with additions and revisions from all authors, and conceived and supervised the project; all authors have read and approved the final version of the article.

www.plantphysiol.org/cgi/doi/10.1104/pp.19.00559

 

mutants of the C3 plants Arabidopsis (*Arabidopsis thaliana*), barley (*Hordeum vulgare*), pea (*Pisum sativum*), and tobacco (*Nicotiana tabacum*) were generated to facilitate the molecular analysis of this important process. These mutants showed the characteristic photorespiratory phenotype, i.e. they could not grow at ambient air conditions but could be rescued in the presence of enhanced $CO_2$ supplementation (e.g. summarized in Blackwell et al., 1988; Leegood et al., 1995; Somerville, 2001; Timm and Bauwe, 2013). More recently, photorespiratory mutants of organisms performing a carbon concentrating mechanism, such as cyanobacteria, red and green algae (Suzuki et al., 1990; Nakamura et al., 2005; Eisenhut et al., 2008; Rademacher et al., 2016), as well as C4 plant species (Zelitch et al., 2009; Levey et al., 2019), were obtained, which also showed the photorespiratory phenotype, supporting the view of photorespiration as an essential partner of photosynthesis in oxygen-rich atmospheres. The detailed physiological and molecular characterization of all these mutants has generated a comprehensive picture of photorespiration, including the biochemical pathway, the underlying genetics, and how photorespiration is embedded in the network of primary metabolism and interacts with many other pathways within the entire cellular context (e.g. reviewed in Wingler et al., 2000; Reumann and Weber, 2006; Foyer et al., 2009; Bauwe et al., 2010, 2012; Fernie et al., 2013; Hodges et al., 2016; Obata et al., 2016; Timm et al., 2016).

In contrast to our broad knowledge on the function of photorespiration, less progress has been made with regards to potential regulatory mechanisms within the photorespiratory cycle. Existing data indicate the mitochondrial Gly-to-Ser conversion, catalyzed through Gly-decarboxylase (GDC) in conjunction with Ser-hydroxymethyltransferase (SHMT1), potentially represents target sites for the regulation of photorespiration. The importance of the GDC and SHMT reactions are based on three facts. First, during Gly-to-Ser conversion, $CO_2$ and ammonia are liberated. Hence, this step of photorespiration emerged as the prime target for genetic engineering approaches to increase crop productivity (Peterhänsel et al., 2013; Betti et al., 2016; Walker et al., 2016; South et al., 2018, 2019). Second, GDC activity is a key component in the control of photosynthesis and plant growth (Timm et al., 2012a, 2015, 2016; Simkin et al., 2017; López-Calcagno et al., 2018). Third, the GDC reaction cycle requires four cooperating proteins, GDC-P, GDC-T, GDC-H, and GDC-L, where GDC-L is also involved in the reaction cycle of other enzymatic complexes, indicating this biochemical activity needs proper regulation (Douce et al., 2001; Timm et al., 2015).

In addition to light-induced transcriptional and translational activation of GDC (Walker and Oliver, 1986; Vauclare et al., 1996; Timm et al., 2013), the GDC activity in plant mitochondria appears to be sensitive to redox changes. The NADH and $NAD^+$ levels especially are of importance given an increased NADH/$NAD^+$ ratio strongly impedes Gly-to-Ser turnover (Bourguignon et al., 1988). Isolated GDC could be also competitively inhibited by Ser ($K_i$ ~4 mM; Oliver and Sarojini, 1987). Finally, GDC activity can be also modulated via posttranslational modification. For example, Palmieri et al. (2010) showed regulation of GDC activity by *S*-nitrosylation and *S*-glutathionylation of GDC-H and GDC-P, respectively. Moreover, Hodges et al. (2013) reported phosphorylation of several GDC proteins and proposed those modifications might contribute to activity regulation. Proteomic analyses provided evidence all four GDC proteins contain conserved Cys residues and therefore might undergo redox-regulation in vivo (Balmer et al., 2004; Keech et al., 2017; Pérez-Pérez et al., 2017). Indeed, it was demonstrated recombinant cyanobacterial GDC P-protein could be activated under reducing conditions (Hasse et al., 2013).

The above-mentioned results make it likely the Gly-to-Ser conversion is modulated via redox-regulation at multiple points. Hence, we investigated whether a mitochondrial thioredoxin (TRXo1) is involved in the potential redox regulation of photorespiratory reactions in this compartment. To this end, we compared the photosynthetic gas-exchange and the metabolic acclimation toward an altered $CO_2$ partial pressure of the transfer DNA (T-DNA) insertional line *trxo1* (*trxo1-1*; Daloso et al., 2015) and a newly generated double mutant (*TxGT*), which is defective in *TRXo1* expression and strongly reduced in the GDC T-protein (*gldt1-1*; Timm et al., 2018). Moreover, we performed in vitro lipoamide dehydrogenase (LPD) activity measurements using isolated mitochondria or recombinant proteins to provide direct experimental evidence for redox-regulation of GDC. Collectively, our results provide evidence TRXo1 is involved in the regulation of mitochondrial photorespiration and thus contributes to the adaptation of the photorespiratory flux toward changes in the environmental conditions that affect the subcellular redox-state.

## RESULTS

### Deletion of *TRXo1* Causes an Increase in the Stoichiometry of Photorespiratory $CO_2$ Release

In general, mutants defective in photorespiration or associated processes exhibit a distinct negative impact on photosynthetic gas exchange (e.g. Timm et al., 2012b; Eisenhut et al., 2013; Pick et al., 2013; Dellero et al., 2015). Apart from constraints within the core cycle, deletion of genes that encode for proteins of accessory functions are characterized by an increase in the stoichiometry of photorespiratory $CO_2$ release, particularly under conditions that require photorespiration to operate at high efficiencies (Cousins et al., 2011; Timm et al., 2011). To test whether *TRXo1* mutation impacts photorespiratory metabolism, the T-DNA insertional line *trxo1* (*trxo1-1*; Daloso et al., 2015) and the wild type were subjected to varying oxygen concentrations (3%, 21%, 40%, and 50% $O_2$) during gas exchange measurements. As shown in Figure 1A, *trxo1* showed no alteration in the net $CO_2$

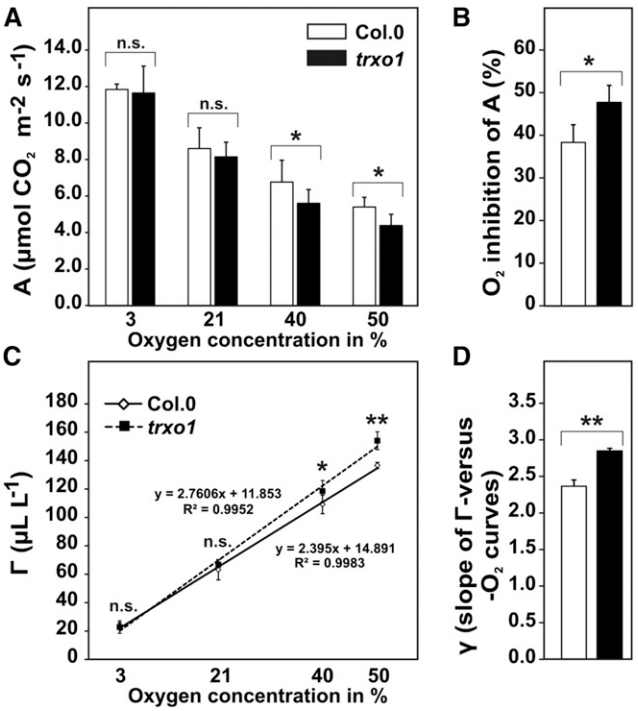


**Figure 1.** Oxygen-dependent gas exchange of *trxo1* and the wild type. Plants were grown in normal air (390 $\mu$L $L^{-1}$ $CO_2$) with a 10-/14-h day/night cycle. After 8 weeks (growth stage 5.1; Boyes et al., 2001), plants were used for gas exchange measurements at varying oxygen concentrations (3%, 21%, 40%, and 50% $O_2$, balanced with $N_2$). Mean values ± SD ($n$ = 5-8) are shown. A, net $CO_2$ uptake rates (A). B, oxygen inhibition of A. C, $CO_2$ compensation points (Γ). D, slopes of the Γ-versus-oxygen concentrations (γ). Asterisks indicate significant alterations of the *trxo1* mutant compared with the wild type according to Student's *t* test (*$P < 0.05$, **$P < 0.01$; n.s., not significant). For details on the calculation of oxygen inhibition and γ, see "Materials and Methods."

assimilation rate (A) at low or normal photorespiratory flux (3% and 21% $O_2$), which was in agreement with unaltered growth in normal air (Daloso et al., 2015) but significantly decreased photosynthesis at enhanced $O_2$ concentrations (40% and 50%), indicating a higher flux through photorespiration. Hence, $O_2$ inhibition of A (Fig. 1B) was significantly higher in *trxo1* (47.7 ± 4.0%) compared with the wild type (38.3 ± 4.1%). In accordance with the decreased A, the $CO_2$ compensation point (Γ) was unchanged at 3% and 21% $O_2$ but was significantly higher in *trxo1* at 40% and 50% $O_2$ (Fig. 1C). These changes increased the slope (γ) from the estimated Γ-versus-oxygen response lines by about 20% (Fig. 1D), indicating a higher fraction of $CO_2$ released from photorespiration.

### Metabolic Effects of *TRXo1* Deficiency on Gly Turnover and Cellular Redox Components

To further substantiate whether mitochondrial localized TRXo1 (Daloso et al., 2015) contributes to mitochondrial photorespiration, we next performed metabolomics during $CO_2$ transition using liquid chromatography coupled to tandem mass spectrometry (LC-MS/MS). Rationally, $CO_2$ concentrations were varied to distinguish between conditions with suppressed [high $CO_2$, high carbon (HC), 1500 $\mu$L $L^{-1}$ $CO_2$, 9 h illumination] and active photorespiration after transferring the plants into normal air (390 $\mu$L $L^{-1}$ $CO_2$, 9 h illumination). For comparison, we included the GDC T-protein knockdown mutant *gldt1*, which is characterized by a ~70% reduction in total GDC activity (*gldt1-1*; Timm et al., 2018).

In agreement with previous studies by Timm et al. (2012b) and Eisenhut et al. (2017), the Gly content (~3.8-fold) and the Gly-to-Ser ratio (~4.2-fold) of the wild type increased 9 h after the transfer into normal air (Fig. 2), whereas other photorespiratory intermediates, such as Ser, glyoxylate, 3-hydroxypyruvate (3-HP), and glycerate, and the CBC-related metabolite 3-PGA were largely unaffected in response to the $CO_2$ concentration decrease used in this study. Furthermore, the redox-related compounds glutathione (GSH), Cys, and cystine also remained unchanged in the wild type after the shift for 9 h into normal air (Fig. 2). Interestingly, the Gly accumulation in *trxo1* was ~10-times (~43-fold) higher after activation of photorespiration when compared with the wild type (Fig. 2). This strong Gly increase was accompanied by a sharp drop in Ser. Furthermore, the photorespiratory intermediates glyoxylate (HC) and glycerate (HC and normal air) showed only minor but significant alterations in *trxo1* when compared with the wild type (Fig. 2). As observed for Ser, 3-PGA, the primary carboxylation product of Rubisco, also significantly decreased in *trxo1* after 9 h in normal air (Fig. 2). Somewhat different from the wild type, the absolute amounts of the redox-related components GSH and Cys, but not cystine, were elevated after 9 h in normal air in *trxo1*. As expected, reduction of GDC activity to ~30% impaired Gly-to-Ser conversion in *gldt1* and thus caused a striking elevation in Gly up to 71-fold after 9 h in normal air compared with HC, a trend that was also observed in GSH, Cys, and cystine levels (Fig. 2). Concerning the other photorespiratory intermediates, an increase was only seen in the upstream intermediate glyoxylate after 9 h in normal air, whereas the downstream pathway metabolites 3-HP and glycerate were invariant at this time point. In accordance to *trxo1*, 3-PGA was also lower in *gldt1* shifted into normal air (Fig. 2). *Trxo1* and *gldt1* showed a comparable and significant decrease in Ser after the shift into normal air, which caused a much stronger increase in the Gly-to-Ser ratios in both mutants than in the wild type (Fig. 2).

Apart from changes in intermediates related to photorespiration and redox buffering, lowering the prevailing $CO_2$ concentration from 1500 to 390 $\mu$L $L^{-1}$ had only a minor impact on metabolite levels of the TCA-cycle in the wild type and *trxo1*. Although several pathway intermediates (e.g. citrate, fumarate) did not show major fluctuations during $CO_2$ transition

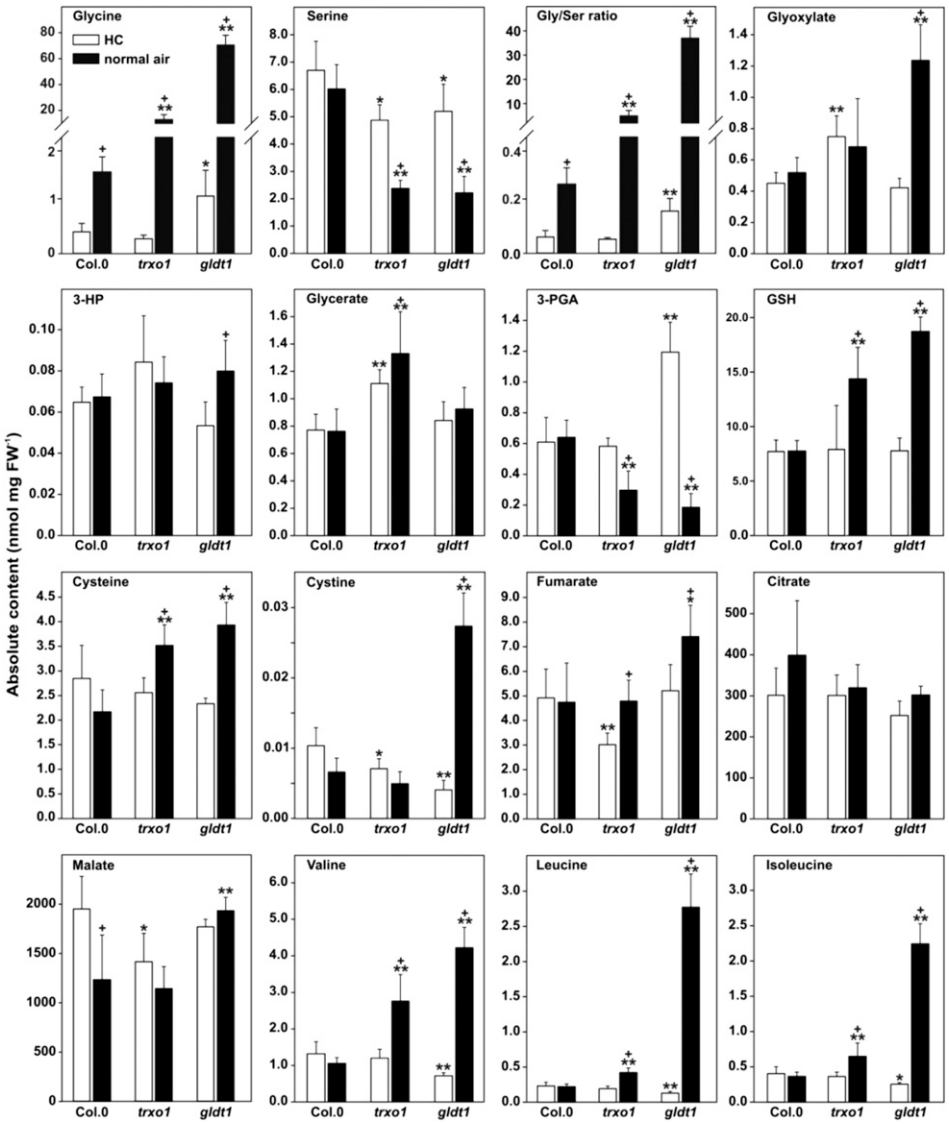


**Figure 2.** Selected metabolites in wild-type, *trxo1*, and *gldt1* plants during $CO_2$ transition. Plants were grown in high $CO_2$ (1500 $\mu$L $L^{-1}$, HC) with a 10-/14-h day/night cycle. After 8 weeks (growth stage 5.1; Boyes et al., 2001), plants were transferred to normal air (390 $\mu$L $L^{-1}$ $CO_2$) with otherwise equal conditions. Leaf-material was harvested in HC (after 9 h of illumination, suppressed photorespiration control) and after transfer into normal air (9 h of illumination, active photorespiration), respectively. Shown are mean values ± SD ($n > 4$) of selected metabolites quantified by LC-MS/MS analysis. Asterisks indicate significant alterations of the mutants compared with the wild type in each condition according to Student's *t* test (*$P <$ 0.05; **$P < 0.01$) and plus signs between HC and normal air values of each genotype ($^{+}P < 0.05$). For the full dataset including statistical evaluation, please see Supplemental Table S1.

in the wild type, a slight decrease in malate and a slight increase in succinate was observed (Fig. 2; Supplemental Table S1). Deletion of *trxo1* also did not cause major and uniform changes in the absolute abundances of metabolites related to the TCA cycle, except for a reduction of malate and fumarate in HC and of succinate in normal air (Fig. 2; Supplemental Table S1). In contrast, *gldt1* accumulated fumarate (~1.6-fold), malate (~1.6-fold), and succinate (4-fold) in normal air, whereas its levels at HC were similar to wild type and *trxo1* (Fig. 2; Supplemental Table S1). Finally, *gldt1* comprised significantly higher amounts of the branched chain (Val, Ile, and Leu) and aromatic (Phe, Trp, and Tyr) amino acids upon the transfer into normal air as previously reported for other photorespiration mutants (Fig. 2; Supplemental Table S1; Timm et al., 2012b; Orf et al., 2016; Eisenhut et al., 2017). Somewhat similar, *trxo1* also increased the level of the branched chain and aromatic amino acids after 9 h in normal air (Fig. 2; Supplemental Table S1). From these results we conclude the most dominant metabolic effect of redox regulation via TRXo1 is on the Gly-to-Ser conversion through GDC/SHMT reactions and, to lesser extent, also on metabolites involved in pathways that require at least one LPD-containing multienzyme system (further discussed in the section "The Double Mutant *TxGT* Shows the Characteristic Photorespiratory Metabolic Signature").

### Lack of *TRXo1* Does Not Affect mRNA Expression and Protein Abundance of Photorespiratory Genes/Proteins

Given the altered Gly-to-Ser conversion in *trxo1* could be due to an altered expression of the enzymes participating in photorespiration, we next analyzed mRNA and protein contents of enzymes involved in the mitochondrial steps of photorespiration. To this end, leaf material of *trxo1* and the wild type was harvested at the end of the day (9 h illumination) in normal air and

reverse transcription-quantitative PCR (RT-qPCR) and immuno-blotting experiments were conducted. As shown in Figure 3, we never observed significant alterations in neither mRNA nor protein levels of all four GDC genes and the major photorespiratory SHMT1 isoform. Similarly, constant expression was also detected in all three genes that served as controls for photorespiratory enzymes not localized in the mitochondrion (Fig. 3), namely peroxisomal hydroxypyruvate reductase 1 (HPR1), peroxisomal malate dehydrogenase (pMDH), and chloroplastic 2-PG phosphatase (PGLP).

### Deletion of *TRXo1* in the *gldt1* Background Intensifies the Photorespiratory Phenotype

Next we hypothesized that if TRXo1 affects GDC activity, phenotypic and physiological alterations would be exacerbated in mutants that exhibit combined defects in *TRXo1* and *GDC* expression under photorespiratory conditions. For this reason, *trxo1* was crossed with the *gldt1* knockdown mutant (5% residual *GDC-T* mRNA expression; Timm et al., 2018) to obtain the double mutant *TxGT* (for genotypic verification see Supplemental Fig. S1). As shown in Figure 4A, wild-type and *trxo1* plants grew similarly (unchanged rosette diameter and leaf number) and were invariant from each other with regard to chlorophyll a fluorescence. In agreement with previous findings (Timm et al., 2018), *gldt1* showed reduced growth (reduction in the rosette diameter), yellowish leaves, and lowered quotient of the variable versus the maximal fluorescence of PSII ($F_v/F_m$) under photorespiratory conditions. Interestingly, the reduction of growth and PSII efficiency observed in the *gldt1* mutant was further enhanced in the *TxGT* line (Fig. 4A). The slower growth of *gldt1* and *TxGT* mutant lines also caused delayed onset of flowering for ~1 and 3 weeks, respectively. If plants were cultivated in HC, suppressing photorespiration, growth of the *gldt1* and *TxGT* lines was fully restored to wild-type levels, as reflected by the unchanged rosette diameter and total leaf number, whereas *TxGT* still showed a significant decrease in $F_v/F_m$ (Fig. 4B). Collectively, $CO_2$-dependent complementation of growth suggests the stronger phenotypic alterations in *TxGT* are due to an additive, negative impact on photorespiration.

### Mutation of *TRXo1* and *GDC-T* Does Not Affect Expression of Photorespiratory Proteins

To exclude the intensified signs of the photorespiratory phenotype due to altered expression of photorespiratory enzymes in the double mutant, we again conducted immunoblot analysis of all mutants in comparison with the wild type in a $CO_2$ transfer

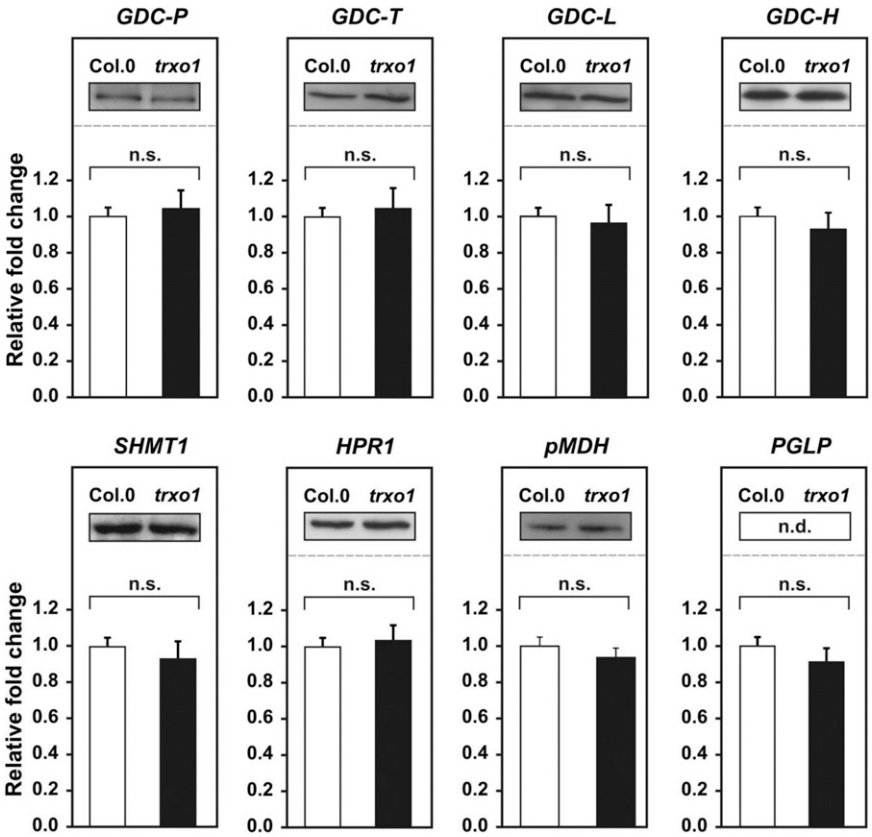


**Figure 3.** Gene and protein expression of selected photorespiratory enzymes. Plants were grown in normal air (390 $\mu$L $L^{-1}$ $CO_2$) with a 10-/14-h day/night cycle. After 8 weeks (growth stage 5.1; Boyes et al., 2001), leaf material was harvested at the end of the day (9 h illumination) and used for subsequent mRNA and protein extraction. Shown are mean values ± SD ($n = 3$) of mRNA expression and representative immunoblots from the *trxo1* mutant compared with the control. n.s., not significant; n.d., not determined.

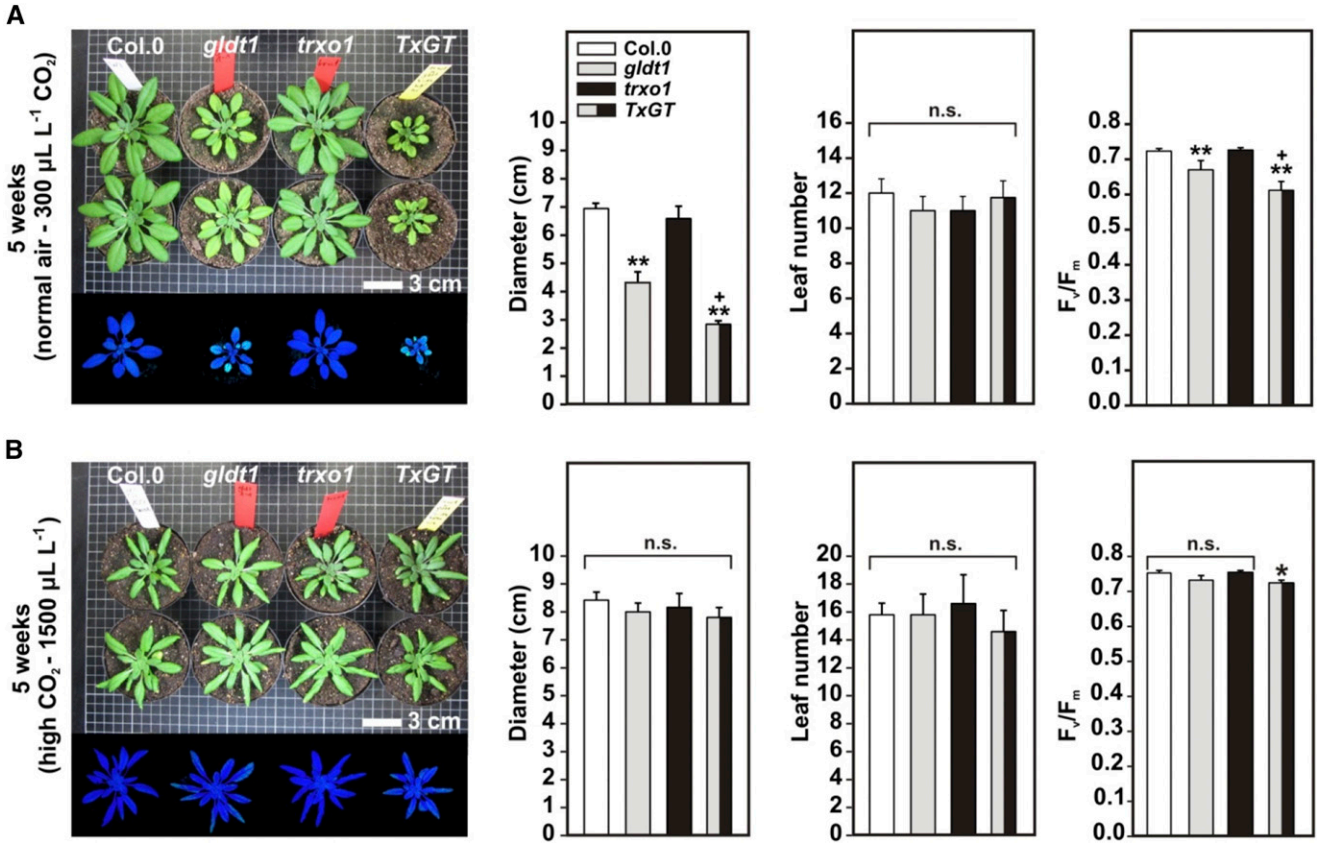


**Figure 4.** Phenotype, growth, and chlorophyll a fluorescence of the *TxGT* double mutant. Plants were grown in normal air (390 $\mu$L L$^{-1}$ $CO_2$; A) or high $CO_2$ (1500 $\mu$L L$^{-1}$, HC; B) with a 10-/14-h day/night cycle. After 5 weeks plants were photographed, rosette diameters and total leaf numbers determined, and chlorophyll a fluorescence measurements conducted. Shown are mean values ± SD ($n > 5$). Asterisks indicate values significantly different from the control (*$P < 0.05$; **$P < 0.01$; n.s., not significant) and plus signs between the *gldt1* single and the *TxGT* double mutant ($^{+}P < 0.05$). Please note that fluorescence images are digitally abstracted and placed in a composite for comparison.

experiment as done for metabolite profiling. To this end, leaf material was harvested from 8-week-old plants in HC (9 h light) and normal air (1 and 9 h light, respectively) and compared with each other. Expression analysis was restricted to the protein level, because mRNA levels of photorespiratory genes were found to be unaffected during $CO_2$ transition previously (Eisenhut et al., 2017). With regard to mitochondrial photorespiration, we did not observe any major and systematic changes in the expression of GDC proteins (P, L, and H) or SHMT1 (Supplemental Fig. S2). Furthermore, other photorespiratory proteins (PGLP and HPR1) as well as RbcL, the E2 subunits of the oxoglutarate dehydrogenase complex (OGDC), and the pyruvate dehydrogenase complex (PDHC) from the TCA-cycle also were unchanged in all genotypes at different $CO_2$ conditions (Supplemental Fig. S2). Thus, this experiment demonstrates that neither the knockdown of *GDC-T* or the knockout of *TRXo1* alone nor the combination of both altered the abundance of photorespiratory core enzymes during $CO_2$ transition.

### The Double Mutant *TxGT* Exhibits Strong Impairment of Photosynthetic $CO_2$ Assimilation

Given the distinct phenotype of the *TxGT* double mutant, its photosynthetic capacity was next characterized in more detail. Due to the smaller leaves of air-grown *TxGT*, which prevented appropriate gas-exchange measurements, plants were first grown in HC for 7 weeks to synchronize growth. After transfer to normal air and acclimation for 1 week, *gldt1*, *TxGT*, and wild-type plants were analyzed. As depicted in Figure 5, values of A, Γ, oxygen inhibition, and $\gamma$ in wild-type plants were similar to plants consequently grown in normal air (see Fig. 2). However, the *gldt1* mutation had a negative impact on $CO_2$ assimilation, which steadily increased during measurements with elevated $O_2$ concentrations. Accordingly, A and Γ of *gldt1* were reduced by about 18% and 14% at low $O_2$ (3%) but by about 58% and 35% in a high $O_2$ (50%) atmosphere, respectively (Fig. 5, A and C). These changes summed up to an ~80% increase in $O_2$ inhibition of A and ~39% of $\gamma$ (Fig. 5, B and D). These alterations were elevated in the *TxGT* plants

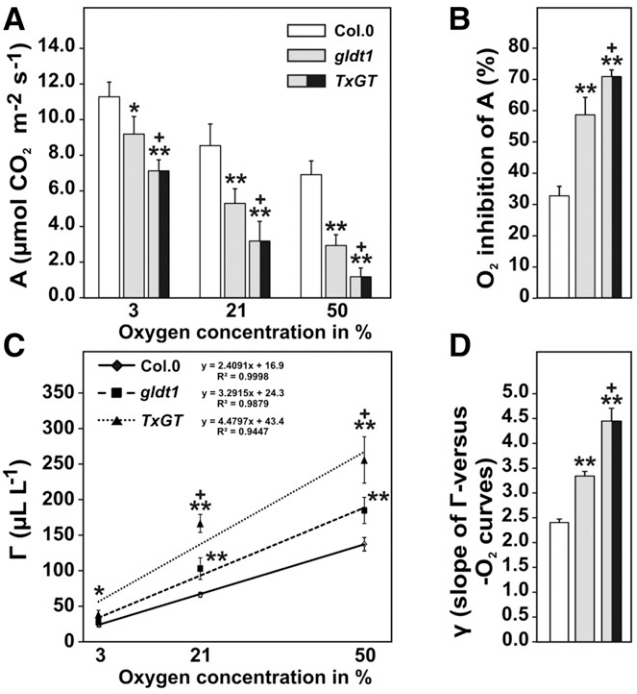


**Figure 5.** Oxygen-dependent gas exchange of *gldt1*, *TxGT*, and the wild type. Plants were grown in high $CO_2$ (1500 $\mu$L $L^{-1}$) with a 10-/14-h day/night cycle. After 7 weeks (growth stage 5.1; Boyes et al., 2001), plants were transferred to normal air (390 $\mu$L $L^{-1}$ $CO_2$) and used for gas exchange measurements at varying oxygen concentrations (3%, 21%, and 50%, balanced with $N_2$) after 1 week acclimation to the altered atmosphere. Mean values ± SD ($n$ = 5–8) are shown for net $CO_2$ uptake rates (A; A), oxygen inhibition of A (B), $CO_2$ compensation points (Γ; C), and slopes of the Γ-versus-oxygen concentrations ($\gamma$; D). Asterisks indicate significant alterations of the mutants compared with the wild type according to Student's $t$ test (*$P < 0.05$, **$P < 0.01$) and plus signs between the *gldt1* single and the *TxGT* double mutant ($^{+}P < 0.05$). For details on the calculation of oxygen inhibition and $\gamma$, see "Materials and Methods."

grown for 1 week in normal air. Hence, a decrease in A (~37%) and an increase in Γ (~57%) were already larger at low $O_2$ and significantly higher at 50% $O_2$ (A - ~83%; Γ - ~86%; Fig. 5, A and C). These inhibitory effects also resulted in increased $O_2$ inhibition of A (~117%) and enhanced $\gamma$ (~85%; Fig. 5, B and D). Collectively, these data suggest an additive, negative impact of both mutations on photorespiration and, in turn, photosynthesis.

### Impairment of Mitochondrial Photorespiration Alters Pyridine Nucleotide Contents

The above-mentioned results provided evidence that *TRXo1* deficiency impacts mitochondrial photorespiration, particularly GDC, which is known to be the major source of NADH production in illuminated leaves (Leegood et al., 1995). Moreover, TRXo1 belongs to the cellular TRX system, which is directly linked to the cellular pyridine nucleotide pools, because NADPH-dependent thioredoxin reductases (NTRs) use NADPH as reducing power for various TRX proteins (Geigenberger et al., 2017). Consequently, we next quantified the abundances of pyridine nucleotides ($NAD^+$, NADH, $NADP^+$, and NADPH) in all genotypes during $CO_2$ transition, with leaf material harvested in HC (9 h illumination) and after the shift into normal air (1 h and 9 h illumination). In HC, we did not observe significant alterations in $NAD^+$, NADH, and the NADH/$NAD^+$ ratio between these genotypes (Fig. 6, A–C), except a slight increase in the NADH/$NAD^+$ ratio in the *TxGT* mutant (Fig. 6C). After the transfer into normal air for 1 h, all mutant genotypes displayed decreased NADH and higher $NAD^+$ abundances (except *gldt1*), leading to significant reductions in the NADH/$NAD^+$ ratio in all mutants when compared with the wild type (Fig. 6, A–C). These changes mostly disappeared after 9 h in normal air, but all mutants consistently showed slightly decreased NADH amounts compared with wild type (Fig. 6, A–C). Comparable changes were observed in the amounts of the phosphorylated pyridine nucleotide abundances. In HC, only the *TxGT* mutant had elevated NADPH and decreased $NADP^+$ levels, whereas the NADPH/$NADP^+$ ratio was higher in the *trxo1* and *TxGT* lines (Fig. 6, D–F). After the transfer to normal air for 1 as well as 9 h, NADPH significantly decreased in all genotypes (Fig. 6D), whereas $NADP^+$ was only transiently elevated in *trxo1* and *TxGT* (Fig. 6E). However, all mutant lines were characterized by a significant decrease in the NADPH/$NADP^+$ ratio at both time points in air (Fig. 6F).

### The Double Mutant *TxGT* Shows the Characteristic Photorespiratory Metabolic Signature

Next we analyzed how the combined mutation of *TRXo1* and *GDC-T* affects the steady-state metabolite profile in *TxGT*. To this end, leaf material from plants consequently grown in either HC (1500 $\mu$L $L^{-1}$ $CO_2$) or normal air (390 $\mu$L $L^{-1}$ $CO_2$) was harvested after 9 h of illumination under both conditions, and selected metabolites were quantified by LC-MS/MS analysis. As shown in Figure 7, Gly was invariant between the wild type and *trxo1* in HC, but it already increased in *gldt1* (~1.7-fold) and *TxGT* (~3.5-fold) under this condition. In normal air, leaves of the wild type and the *trxo1* mutant contained similar amounts of Gly compared with HC. However, a much stronger increase in Gly was observed in leaves of *gldt1* (~17-fold) and especially *TxGT* (~54-fold) under normal air conditions. These changes, together with the largely unaltered Ser amounts in all plant lines, also caused a significant elevation of the cellular Gly-to-Ser ratio. Only in *gldt1* and *TxGT* was it already higher at HC (~1.7- and ~2.5-fold) and increased further in normal air (~13.8- and ~43.5-fold) conditions.

Other photorespiratory intermediates did not significantly change between the genotypes after growth

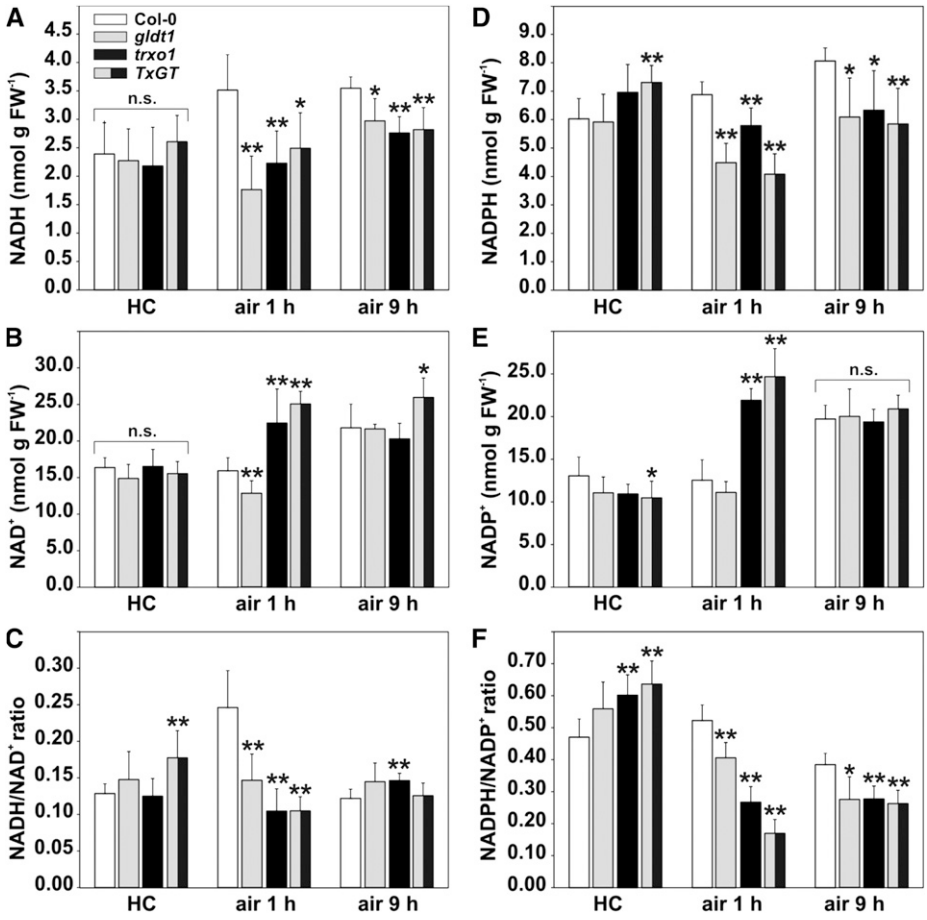


**Figure 6.** Pyridine nucleotide contents in wild-type, *gldt1*, *trxo1*, and *TxGT* plants during $CO_2$ transition. Shown are NADH (A), $NAD^+$ (B), NADH/$NAD^+$ ratio (C), NADPH (D), $NADP^+$ (E), and NADPH/$NADP^+$ ratio (F). Plants were grown in high $CO_2$ (1500 $\mu$L $L^{-1}$, HC) with a 10-/14-h day/night cycle. After 8 weeks (growth stage 5.1; Boyes et al., 2001), plants were transferred to normal air (390 $\mu$L $L^{-1}$ $CO_2$) with otherwise equal conditions. Leaf material was harvested in HC (9 h light) and in normal air (1 and 9 h light). Shown are mean values ± SD ($n > 6$) of pyridine nucleotides ($NAD^+$, NADH, $NADP^+$, and NADPH) quantified by spectrophotometric analysis. Asterisks indicate significant alterations of the mutants compared with the wild type according to Student's *t* test. $^*P < 0.05$, $^{**}P < 0.01$. FW , fresh weight; n.s., not significant.

in HC, except a slight increase in 3-HP in the *TxGT* mutant. Under ambient air conditions, however, we found elevated amounts of glyoxylate (significant in *gldt1* and *TxGT*) and decreased amounts of glycerate (all lines) and 3-PGA (significant in *trxo1* and *TxGT*) in the mutants compared with the wild type (Fig. 7). Only 3-HP did not follow this trend given its content was slightly higher in *trxo1* and *TxGT*. The compounds related to the redox-homeostasis were also analyzed in this experiment and compared with the results shown in Figure 2. Except a slight increase in GSH and Cys in *TxGT*, all three compounds were basically unaltered between the other genotypes and the wild type under HC conditions (Fig. 7). Growth in normal air significantly changed the amounts of all three intermediates. In the wild type, GSH, Cys, and cystine were lower compared with HC (Fig. 7). In the mutants, however, all three intermediates showed gradually increased amounts in the order of their negative impact on photorespiration (*trxo1* < *gldt1* < *TxGT*).

Apart from these changes, several other metabolic alterations previously observed in *trxo1* (Fig. 2; Supplemental Table S1) and *gldt1* (Timm et al., 2018) were much more pronounced in the *TxGT* double mutant (Supplemental Table S2). For example, *TxGT* accumulated higher amounts of the branched chain amino acids Val (~2.7-fold), Ile (~4.2-fold), and Leu (~9.1-fold) as well as the aromatic amino acids Phe (~4.2-fold), Trp (~5.5-fold), and Tyr (~6.6-fold) in normal air compared with the wild type (Fig. 7; Supplemental Table S2). Enhanced accumulation was also seen for Pro, His, Arg, and Asn, whereas Ala and Asp were strongly decreased in *TxGT*. Finally, changes were also observed in the amounts of some TCA-cycle intermediates. For example, malate (~2.0-fold) and citrate (~3.6-fold) were elevated, whereas fumarate (~16% of the wild type) was decreased (Fig. 7; Supplemental Table S2). Despite the fact that malate and fumarate are known to accumulate to high levels in the vacuole, changes in their total cellular levels are symptomatic of those observed in response to genetic perturbation in photorespiration (Timm et al., 2012b; Orf et al., 2016). This is likely because the close interaction of the processes of photosynthesis, photorespiration, and respiration as recently discussed (Obata et al., 2016). Mechanistically, due to suboptimal conversion of metabolites through photorespiration and, thus, feedback inhibition of the CBC, increases in malate and fumarate could be explained as transient accumulation of photo-assimilates stored in the vacuole to somewhat circumvent impaired carbon export from photosynthesis after a switch from high $CO_2$ to normal air. In summary, the combined mutation of *Trxo1* and

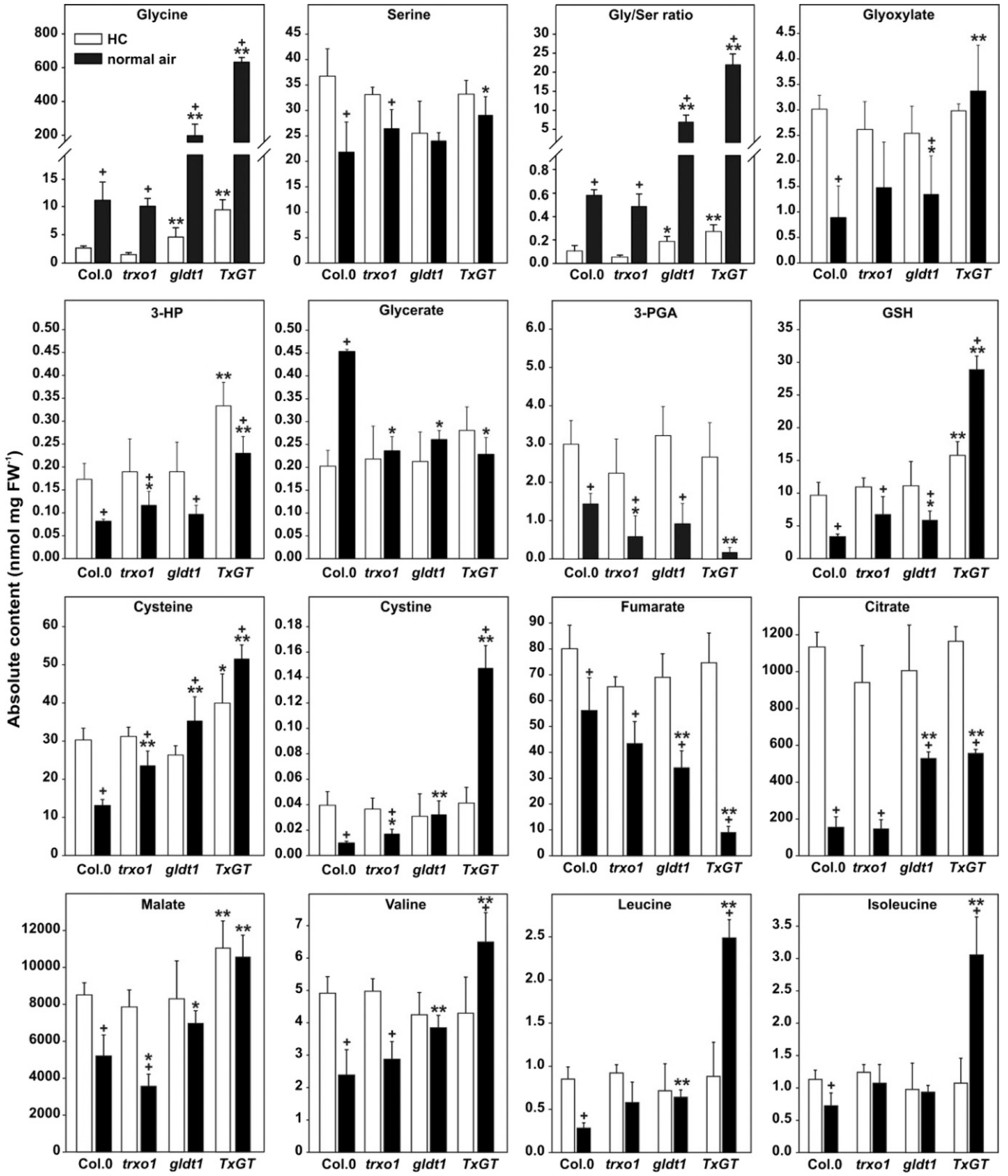


**Figure 7.** Levels of selected metabolites in leaves of the wild type, *trxo1*, *gldt1*, and *TxGT* mutants grown in HC and normal air. Plants were grown in high $CO_2$ (1500 $\mu$L $L^{-1}$, HC) and normal air (390 $\mu$L $L^{-1}$ $CO_2$) with a 10-/14-h day/night cycle. After 8 weeks (growth stage 5.1; Boyes et al., 2001), leaf material was harvested in both conditions after 9 h illumination. Shown are mean values ± SD ($n > 4$) of selected metabolites quantified by LC-MS/MS analysis. Asterisks indicate significant alterations of the mutants compared with the wild type in each condition according to Student's *t* test (*$P < 0.05$; **$P < 0.01$) and plus signs

*GDC-T* enhanced the negative impact on GDC activity and caused a metabolic signature comparable with that observed with other mutants showing a strong photorespiratory phenotype (Timm et al., 2012b; Orf et al., 2016; Eisenhut et al., 2017; Levey et al., 2019).

### Redox-Regulation of the GDC L-Protein from Pea and *Synechocystis* through TRXo1

Given GDC expression was unchanged in *trxo1* and the *TxGT* double mutant (Fig. 3; Supplemental Fig. S2), only alterations in GDC activity could account for the altered Gly accumulation in the mutants. Because H-protein is not enzymatically active and we also observed stronger negative impacts on GDC performance in the double mutant with very low GDC-T amounts, we next tested if the GDC-L protein (LPD) activity can be redox-regulated. For this purpose, activity measurements were carried out using LPD from three different sources, namely isolated pea leaf-mitochondria (native mtLPD), recombinant mtLPD from pea (PsmtLPD), and recombinant LPD from the cyanobacterium *Synechocystis* PCC 6803 (SyLPD) produced and purified after heterologous expression in *Escherichia coli*. As shown in Figure 8, LPD activity from all sources was clearly inhibited upon addition of the artificial reducing agent dithiothreitol (DTT). Its activity decreased by about ~43% (native mtLPD; Fig. 8A), ~52% (PsmtLPD; Fig. 8B), and ~15% (SyLPD; Fig. 8C). Reduction in LPD activity (~35%, ~31%, and ~32%) for native mtLPD, PsmtLPD, and SyLPD, respectively) was also caused through addition of the natural reductant TRXo1 in combination with the NADPH-dependent thioredoxin reductase a (NTRa). Notably, the observed inhibition was due to the activity of the TRXo1/NTRa redox-couple, since no alterations in LPD activity were observed with inactive TRXo1/NTRa (Fig. 8). In summary, these experiments provided evidence that LPD of the plant and cyanobacterial GDC undergoes redox-regulation.

Finally, to pinpoint critical amino acid residues in the LPD proteins used during this study (pea and *Synechocystis*), we analyzed the respective protein sequences in more detail and in comparison with other plant [Arabidopsis and maize (*Zea mays*)] and bacterial (*Azotobacter vinelandii*, *E. coli*, and *Pseudomonas putida*) representatives. Rationally, the presence of conserved Cys residues could help to explain a functional mechanism that might involve disulfide bond formation through TRX proteins, presumably TRXo1. All of the analyzed LPD sequences contain two conserved Cys residues (Cys 45 and Cys 50;

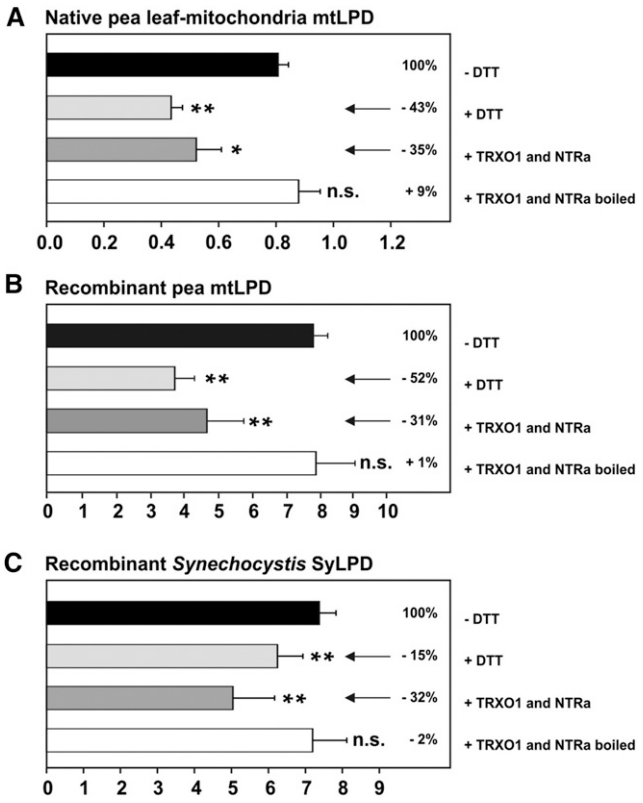


**Figure 8.** Redox-regulation of LPD from pea and Synechocystis. The activity of LPD proteins was determined in extracts of pea leaf-mitochondria or of recombinant proteins produced through heterologous expression in *E. coli* (A) and affinity purification from pea (B) or *Synechocystis* (C). Shown are mean values ± SD ($n > 4$) of LPD activity without or after addition of DTT and recombinant native or boiled TRXo1 and NTRa. Asterisks indicate significant alterations to the control according to Student's *t* test * $P < 0.05$, ** $P < 0.01$; n.s., not significant. For experimental details, see "Material and Methods."

Supplemental Fig. S3). Previous work has suggested that these residues form a disulfide bond that is involved in FAD-binding and might be of further importance for the interaction with the GDC-H protein (Faure et al., 2000). Therefore, we conclude that TRXo1, and perhaps other TRX proteins, could potentially form or split the disulfide bond between Cys 45 and Cys 50 to redox-regulate LPD activity.

## DISCUSSION

Photorespiration has attracted major interest in plant research and is currently one of the major targets in plant breeding (Peterhänsel et al., 2013; Betti et al., 2016; Walker et al., 2016; South et al., 2018, 2019). However, regulatory aspects of photorespiration have been only

**Figure 7.** (*Continued.*)
between HC and normal air values of each genotype ($^{+}P < 0.05$). For a more comprehensive dataset including statistical evaluation, please see Supplemental Table S2. FW, fresh weight.

scarcely investigated. To date, no protein with regulatory impact on photorespiration was identified either via classic randomized mutation screens (Somerville, 2001; Badger et al., 2009) or other procedures (Carroll et al., 2015). The failure to identify regulatory candidates by these strategies could be explained by the fact that regulatory mutants might display a rather weak photorespiratory phenotype or that those proteins are often encoded by redundant gene families (Somerville, 2001; Timm and Bauwe, 2013). Nevertheless, there are several hints that some photorespiratory steps, such as GDC in the mitochondrion, might be prone to redox regulation (Balmer et al., 2004; Keech et al., 2017; Pérez-Pérez et al., 2017). Accordingly, we used a T-DNA insertional mutant that lacks the mitochondrial *TRXo1* (Daloso et al., 2015) to analyze its potential contribution to redox-regulation of photorespiration.

### *TRXo1* Contributes to Photorespiratory Metabolism

The *trxo1* single mutant provides some evidence this protein could indeed be involved in redox-regulation of photorespiration. As such it is perhaps unsurprising it shows an increase in the stoichiometry of photorespiratory $CO_2$ release, which was also previously observed in other mutants with a moderately constrained photorespiratory flux (Cousins et al., 2011; Timm et al., 2011). Further support that TRXo1 impacts mitochondrial photorespiration was provided from our metabolite analysis (Fig. 2). Although rather minor changes in the Gly-to-Ser conversion were observed if *trxo1* was consequently grown in normal air (Fig. 7; Daloso et al., 2015), clear differences in Gly accumulation occurred if the mutant was shifted from HC into normal air to simulate quick photorespiratory activation (Fig. 2). Hence, *TRXo1* mediated regulation could play a more dominant role in the short term acclimation of photorespiration to fluctuating environments that affect photorespiration, such as $CO_2$ concentrations, light intensities, or temperature. In wild-type leaf material, Gly content was low under HC conditions but increased (~3.8-fold) after 9 h in normal air. This increased Gly accumulation after induction of photorespiration is consistent with previous reports (Timm et al., 2012b; Orf et al., 2016; Eisenhut et al., 2017) and points to the necessity that Gly turnover via GDC might need some activation after $CO_2$ shifts. Interestingly, a much more pronounced accumulation of Gly was found in *trxo1* after the shift into normal air. This result suggests that lack of TRXo1 causes a further impairment or slowdown of GDC activity/activation due to a mechanism that involves redox-regulation of mitochondrial photorespiration. A likely candidate for the TRXo1-mediated redox regulation of GDC is mtLPD since its activity decreases when reduced via this protein (Fig. 8, discussed in the paragraph "TRXo1 contributes to redox-regulation of GDC through LPD" in detail). It can thus be anticipated that absence of TRXo1 leads to inappropriate regulation of mtLPD and overall GDC operation that ultimately caused oxidative stress in plant mitochondria. Indeed, we observed that the *trxo1* mutant accumulates the redox-stress–related intermediates GSH and Cys after the shift to normal air (Fig. 2). In agreement, the *gldt1* mutant, which exhibits a direct reduction in the total GDC activity of up to 70% (Timm et al., 2018), displayed a further intensification of the effects observed with *trxo1* (Fig. 2). Any, malfunctioning of GDC reduces NADH regeneration and in turn leads to an undersupply of the respiratory chain. This assumption was supported by our quantification of pyridine nucleotide contents during $CO_2$ transition, which revealed a higher NADH/$NAD^+$ ratio in the wild type (Fig. 6) in agreement with a higher photorespiratory flux through GDC and thus increased NADH production. In contrast, impairment of GDC activation/activity in both *trxo1* and *gldt1* causes a distinct drop in the NADH/$NAD^+$ ratio (Fig. 6). However, these results provide clear evidence that proper GDC regulation is crucial to maintain the cellular redox-homeostasis. Imbalances, particularly in mitochondria, eventually cause higher production of reactive oxygen species (ROS) that might be counteracted via the accumulated GSH (Fig. 2).

However, the observed effects of the single *TRXo1* mutation on photorespiration and related metabolites are rather weak under standard conditions. Such a behavior has been predicted for other regulatory mutants (Timm and Bauwe, 2013). Moreover, TRXo1 is not the only mitochondrial TRX in Arabidopsis. It is known that TRXh2 is also present in mitochondria (Daloso et al., 2015), and we currently cannot rule out some redundancy between these two proteins, thus weakening the phenotype of the single *trxo1* mutant. Interestingly, da Fonseca-Pereira et al. (2019) reported that loss of TRXh2 also impacts photorespiration and is also able to redox-regulate LPD. Given changes in the phosphorylated pyridine nucleotide contents during $CO_2$ transition are most dominant in the *trxo1* and *TxGT* mutants shortly after transfer into normal air (Fig. 6, D–F), it is likely the decrease of the NADPH/$NADP^+$ ratio can only be partially referred to the feedback inhibition on photosynthesis, particularly the CBC, in response to malfunctioning of photorespiration (Timm et al., 2016). The stronger, intermitted responses in mutants lacking TRXo1 could also lead to activation of other TRX proteins that require a higher NADPH turnover through NTRa. Hence, TRXh2 might, at least to some extent, compensate for the loss of TRXo1. Indeed, similar observations have been made with several TRX target enzymes of the TCA-cycle (Daloso et al., 2015), and future research on multiple mutants is needed to precisely elucidate the interplay between the different TRX proteins and their regulation of GDC.

### Lack of *TRXo1* in a *GDC-T* KnockDown Mutant Intensifies the Photorespiratory Phenotype

To further substantiate the impact of TRXo1 on mitochondrial photorespiratory metabolism, we

took advantage of a double mutant approach. For this purpose, *trxo1* was crossed into the *gldt1* background to follow how plant metabolism adapts if overall GDC capacity is decreased to about 70% (*gldt1*; Timm et al., 2018) and additionally lacks the possible TRXo1 mediated redox-regulation. The double mutant *TxGT* showed a more strongly pronounced photorespiratory phenotype than *gldt1.* Growth, PSII activity, and photosynthetic $CO_2$ assimilation were clearly diminished when cultivated in normal air but remained unaltered if grown in HC (Figs. 4 and 5). These changes provide strong evidence that the *TRXo1* and *GDC-T* mutations are negatively additive for photorespiratory metabolism in mitochondria, i.e. the double mutant *TxGT* clearly amplifies the importance of TRXo1 for photorespiration. This finding could indicate that the absence of TRXo1 further decreases the GDC activity but not necessarily through affecting the cellular redox-state as evident by similar changes in the pyridine nucleotide contents between the *trxo1* and the *TxGT* mutant (Fig. 6). In this scenario, activity regulation of GDC could occur directly only on GDC-P or GDC-L, since GDC-H is not enzymatically active and GDC-T is already highly diminished. This assumption is underpinned by the massive increases in Gly and the Gly-to-Ser ratio (Fig. 7), indicating intensified impairment of GDC.

The intensified photorespiratory phenotype can potentially also be explained by missing TRXo1-mediated redox-regulation of other processes, indirectly affecting the operation of GDC. It has been shown that the *trxo1* mutant exhibits a deregulated TCA cycle (Daloso et al., 2015), which in turn could affect photorespiration due to their physiological interaction (Obata et al., 2016). Changes in some TCA cycle intermediates are obvious in the *trxo1* mutant (Supplemental Table S1) and are intensified in the case of malate, citrate, and fumarate in the *TxGT* double mutant (Fig. 7; Supplemental Table S2). Moreover, the TRXo1-mediated regulation of mtLPD (Fig. 8) is not only relevant for the regulation of GDC activity, because this protein in also part of the PDHC and OGDC involved in the TCA cycle, as well as the branched-chain 2-oxoacid dehydrogenase complex (BCDHC) involved in the degradation of branched chain amino acids (Oliver et al., 1990; Millar et al., 1998; Timm et al., 2015). Hence, one might speculate that the strongly enhanced photorespiratory phenotype of the *TxGT* plants is partially related to the malfunction of mtLPD in these multiple complexes. Indeed, in support of this theory some characteristic changes in the TCA-cycle and branched chain amino acid metabolism were visible in *trxo1* and *TxGT* under both HC and normal air (Figs. 2 and 7; Supplemental Tables S1 and S2). The above facts notwithstanding, the phenotypic complementation of *TxGT* by elevated $CO_2$ levels clearly indicates that the main cause of the phenotype is due to a photorespiratory defect. As indicated by the massively elevated Gly amounts, this is presumably mediated by an effect on the GDC activity (Fig. 7).

### TRXo1 Contributes to Redox-Regulation of GDC through LPD

As mentioned above, all four GDC (P, T, H, and L) proteins contain conserved Cys residues and, thus, have been suggested to undergo redox-regulation (Balmer et al., 2004; Keech et al., 2017; Pérez-Pérez et al., 2017). To date, a redox-regulation mechanism was proposed and experimentally verified only for the *Synechocystis* GDC P-protein (Hasse et al., 2013), the actual Gly decarboxylase. It has also been shown that the entire GDC activity became severely inhibited in a more oxidized and reactive oxygen species–producing mitochondrion due to a defect in the endoplasmic reticulum–localized adenylate transporter 1 (*ER-ANT1*) in Arabidopsis and rice (*Oryza sativa*; Hoffmann et al., 2013; Zhang et al., 2016), which was partly relieved upon DTT addition (Hoffman et al., 2013). These findings stimulated us to test GDC-L (mtLPD) for its potential to undergo redox-regulation, which could be based on disulfide bond formation that has been in silico predicted onto the LPD structure (Faure et al., 2000). Accordingly, all LPD proteins possess conserved Cys residues (Cys 45 and Cys 50; Supplemental Fig. S3) that are likely involved in the binding of the FAD-cofactor and crucial for the interaction with GDC-H (Faure et al., 2000). There are further Cys residues that are only conserved in LPD proteins from phototrophic organisms, which we currently assume to play a role in TRX-based diurnal LPD redox-regulation. In the course of our experiments, reducing conditions inhibited LPD activity, including native LPD from pea leaf-mitochondria and recombinant proteins from pea and *Synechocystis* PCC 6803. In more detail, the activity of LPD is significantly decreased upon addition of DTT, as well as by the natural redox-couple consisting of the recombinant mitochondrial TRXo1 and NTRa from Arabidopsis (Laloi et al., 2001; Reichheld et al., 2005; Daloso et al., 2015). Redox-regulation of LPD has also been recently suggested in experiments to characterize the thioredoxome of *Chlamydomonas reinhardtii* (Pérez-Pérez et al., 2017). As mentioned before, such a regulation is anticipated to not only affect GDC but also the other mitochondrial enzyme complexes in which LPD is involved, namely, PDHC, OGDC, as well as branched-chain 2-oxoacid dehydrogenase complex. Notably, some of the analyzed organic acids involved in the TCA-cycle (succinate and fumarate) as well as the branched chain (Val, Ile, and Leu) but not the aromatic (Tyr, Phe, and tryptophane) amino acids showed a similar accumulation pattern in *trxo1* during $CO_2$ transition as Gly does (Figs. 2 and 7; Supplemental Tables S1 and S2). Collectively, our results indicate that TRXo1 contributes to the regulation of several mitochondrial multienzyme systems, particularly GDC, in response to environmental fluctuations and thus is involved in the balancing of the overall cellular redox-homeostasis.

## MATERIAL AND METHODS

### Plant Material and Growth

Arabidopsis (*Arabidopsis thaliana*) ecotype Columbia-0 (Col-0) was used as the wild type during this study. T-DNA insertional lines *trxo1-1* (SALK 042792) and *gldt1-1* (WiscDSLox 366A11-085) in the Col-0 background were obtained from the Nottingham Arabidopsis Stock Centre (Alonso et al., 2003; Woody et al., 2007) and homozygous lines produced as described previously (Daloso et al., 2015; Timm et al., 2018). After sterilization with chloric acid, seeds were sown on a soil/vermiculite mixture (4:1), incubated at 4°C for 2 d to break dormancy, and grown under controlled environmental conditions as follows: 10-h day, 20°C/ 14-h night, 18°C, ~120 $\mu$mol photons $m^{-2}$ $s^{-1}$ light intensity, and 70% relative humidity. Where specified in the text, the $CO_2$ concentration was increased from 390 $\mu$L $L^{-1}$ (normal air) to 1500 $\mu$L $L^{-1}$ (HC) with otherwise equal conditions. Plants were regularly watered and fertilized weekly (0.2% [v/v] Wuxal, Aglukon).

### Generation and Verification of the *TRXo1* and *GLD-T* Double Mutant (*TxGT*)

The *trxo1-1* and *gldt1-1* T-DNA insertional lines were crossed to obtain a *trxo1-1-gldt1-1* double mutant (*TxGT*). To verify the T-DNA insertions in both genes in the following generations, leaf DNA was isolated according to standard protocols and PCR amplified (min at 94°C, 1 min at 58°C, 2 min at 72°C; 35 cycles) with primers specific for the left border (R497 for WiscDsLox line, *gldt1-1* or T5 for SALK 042792 line, *trxo1-1*) and *AtGDC-T* (R490) and *TRXo1* (T4) specific primers. The resulting fragments (*gldt1-1* 1859 bp, *trxo1-1* 2000 bp) were sequenced for verification of the T-DNA fragment within both genes. Zygosity was examined by PCR amplification (min at 94°C, 1 min at 58°C, 2 min at 72°C; 35 cycles) of leaf DNA with the primer combination R498 and R490 for *GLD-T* (1943 bp) and T3 and T4 for *TRXo1* (min at 94°C, 1 min at 58°C, 2 min at 72°C; 35 cycles). For oligonucleotide sequences see Supplemental Table S3.

### RT-qPCR Expression Analysis and Immunological Studies

To extract total leaf RNA and protein, plant material (~100 mg) was harvested from normal air-grown wild-type and *trxo1-1* plants at growth stage 5.1 (Boyes et al., 2001) after 9 h of illumination or during the $CO_2$ transfer experiment (Fig. 2; Supplemental Fig. S2) and stored at −80°C until further processing. RNA isolation was carried out using the Nucleospin RNA plant kit (Macherey-Nagel). Following PCR verification of absence of DNA contamination, complementary DNA (cDNA) was synthesized from 2.5 $\mu$g of leaf RNA using the RevertAid cDNA synthesis kit (MBI Fermentas). Prior RT-qPCR analysis cDNA amounts were precalibrated by conventional RT-PCR using signals of the constitutively expressed 40S ribosomal protein *S16* gene. RT-qPCR of selected photorespiratory genes (*GLD-P1*, *GLD-T*, *GLD-H*, *GLD-L1*, *SHMT1*, *HPR1*, *pMDH1*, and *PGLP*; for sequences see Supplemental Table S3) was performed on the LightCycler 1.5 system (Roche) and SYBR Green fluorescence (Roche) for detection as described previously by Timm et al. (2013). To obtain total leaf-protein, plant material was homogenized and extracted in 200 mL of extraction buffer containing 50 mM HEPES-KOH (pH 7.6), 10 mM NaCl, 5 mM $MgCl_2$, 100 mM sorbitol, and 0.1 mM phenylmethylsulfonyl fluoride. After centrifugation (4°C, 10 min, 20,000 *g*), the protein concentration of the supernatant was determined according to Bradford (1976). Subsequently, 10 $\mu$g leaf proteins were separated via SDS-PAGE and transferred onto a polyvinylidene difluoride membrane according to standard protocols. Antibodies of selected photorespiratory proteins (pMDH1, GLD-P, GLD-T, GLD-H, GLD-L, SHMT1, HPR1, and PGLP; Pracharoenwattana et al., 2007; Timm et al., 2013; Flügel et al., 2017) were used to estimate their abundances in the mutant lines and the wild type.

### Gas Exchange and Chlorophyll a Fluorescence Measurements

Leaf gas exchange measurements were performed using fully expanded rosette leaves of plants at growth stage 5.1 (Boyes et al., 2001) with the following conditions: photon flux density = 1000 $\mu$mol $m^{-2}$ $s^{-1}$, chamber temperature = 25°C, flow rate = 300 $\mu$mol $s^{-1}$, and relative humidity = 60 to 70%. For $A/C_i$ curves $CO_2$ steps were 400, 300, 200, 100, 50, 0, and 400 $\mu$L $L^{-1}$. Changes in the $O_2$ concentrations to 3%, 40%, or 50% (balanced with $N_2$) were generated via the gas-mixing system GMS600 (QCAL Messtechnik). Oxygen inhibition of A was calculated from measurements at 21% and 50% oxygen using the equation: $O_2$ inhibition = $(A_{21} - A_{50})/A_{21} \times 100$. Calculation of $\gamma$ was performed by linear regression of the Γ-versus-oxygen concentration curves and given as slopes of the respective functions. Simultaneously, chlorophyll a fluorescence was determined on a pulse-amplitude-modulation fluorometer (DUAL-PAM-100; Walz). Maximum quantum yields of PSII were determined after dark adaptation of the plants for at least 15 min.

### Metabolite Analysis

For LC-MS/MS analysis, leaf material was harvested from fully expanded rosette leaves (sampling time points are specified in the legends of Figs. 2 and 7) of plants at growth stage 5.1 (Boyes et al., 2001), immediately frozen in liquid nitrogen, and stored at −80°C until analysis. Extraction of soluble primary intermediates was carried out using LC-MS grade chemicals according to the method described in Arrivault et al. (2009, 2015) with some modifications. Briefly, ~50 mg leaf-tissue was ground to a fine powder and extracted in 500 $\mu$L of ice-cold LC-MS/MS buffer [150 $\mu$L chloroform, 350 $\mu$L methanol, 1 $\mu$L of MES as internal standard (1 mg/mL)]. Following addition of 400 $\mu$L ice-cold water, samples were vortexed thoroughly and incubated for at least 2 h at −20°C. After centrifugation (10 min, 20,000 *g*, 4°C), the aqueous phase was transferred to a new tube and 400 $\mu$L of ice-cold water again added to the extraction tube. Following stirring and centrifugation (5 min, 20,000 *g*, 4°C), supernatants were combined and lyophilized. Next, the dried extracts were dissolved in 400 $\mu$L water and filtrated through 0.2 $\mu$m filters (Omnifix-F, Braun, Germany). The cleared supernatants were analyzed using the high performance liquid chromatograph mass spectrometer LCMS-8050 system (Shimadzu) and the incorporated LC-MS/MS method package for primary metabolites (version 2, Shimadzu). In brief, 1 $\mu$L of each extract was separated on a pentafluorophenylpropyl column (Supelco Discovery HS FS, 3 $\mu$m, 150 × 2.1 mm) with a mobile phase containing 0.1% (v/v) formic acid. The compounds were eluted at 0.25 mL $min^{-1}$ using the following gradient: 1 min 0.1% (v/v) formic acid, 95% *Aqua destillata* (*A. dest.*), 5% acetonitrile, within 15 min linear gradient to 0.1% (v/v) formic acid, 5% *A. dest.*, 95% acetonitrile, 10 min 0.1% (v/v) formic acid, 5% *A. dest.*, 95% acetonitrile. Aliquots were continuously injected in the MS/MS part and ionized via electrospray ionization. The compounds were identified and quantified using the multiple reaction monitoring values given in the LC-MS/MS method package and the LabSolutions software package (Shimadzu). Authentic standard substances (Merck) at varying concentrations were used for calibration and peak areas normalized to signals of the internal standard. Glyoxylate, 3-HP, and glycerate were determined in the negative ion mode using selective ion monitoring for *m/z* 73, 102, and 105 corresponding to the deprotonated glyoxylate, 3-HP, and glycerate ions $[M\text{-}H]^-$. Retention time acquisition window (2 min) was verified with coelution experiments using purchased glyxoylate, 3-HP, and glycerate (Sigma-Aldrich). Varying concentrations of the three metabolites were also used for calibration curves. Data were interpreted using the Lab solution software package (Shimadzu).

### Determination of Pyridine Nucleotide Contents

The contents of $NAD^+$/NADH and $NADP^+$/NADPH were determined in acid and alkaline extracts using the protocol described in Queval and Noctor (2007). The assays involve the phenazine methosulfate-catalyzed reduction of dichlorophenolindophenol in the presence of ethanol and alcohol dehydrogenase (for $NAD^+$ and NADH) or Glc-6-P and Glc-6-P dehydrogenase (for $NADP^+$ and NADPH). Reduced and oxidized forms are distinguished by preferential destruction through measurements in acid or alkaline buffers.

### Cloning, Expression, and Purification of Recombinant Enzymes

To express cyanobacterial and plant LPDs, the open reading frames were PCR amplified from *Synechocystis species* strain PCC 6803 genomic DNA (SyLPD; *slr1096*; 1096XhoI-fw/1096EcoRI-rev) or pea (*Pisum sativum*; PsmtLPD; P454/P294) cDNA and ligated into the pGEMT vector (Invitrogen) for amplification and sequencing (Seqlab). The respective fragments were excised using the introduced restriction sites (SyLPD – *Xho*I/*Eco*RI and PsmtLPD – *Bam*HI/*Eco*RI) and ligated into vector pBADHisA (Invitrogen) or pET28a (Novagene) pBADHisA (Invitrogen) to obtain pBADHisA-SyLPD and pET28a-*Ps*mtLPD. Expression vectors pET16b-AtTRXo1 and pET16b-AtNTRa were generated as

described previously (Laloi et al., 2001). Overexpression of the four constructs was carried out in 200 mL Luria-Bertani medium containing ampicillin (200 $\mu$g mL$^{-1}$) for the pBADHisA and pET16b or kanamycin (100 $\mu$g mL$^{-1}$) for the pET28a vectors. Overexpression cultures were inoculated with 1 mL of a freshly prepared overnight culture (~16 h) and shaken (200 rpm) at 37°C until optical density at 600 nm ($OD_{600}$) = ~0.6. Expression in *Escherichia coli* was carried out as follows: pBADHisA:SyLPD, strain LMG194, induction with 0.2% (w/v) arabinose, and incubation at 30°C (200 rpm) for ~16 h, or pET28a and pET16b, strain BL21, induction with isopropylthio-$\beta$-galactoside (1 mM), and incubation at 37°C (200 rpm) for 4 h (AtTRXo1 and AtNTRa) or 30°C for ~16 h (PsmtLPD1). The cells were harvested and resuspended in 20 mM TrisHCl, pH 8.0, containing 300 mM NaCl, and 20 mM Imidazol. Next, lysozyme was added (1 mg/mL) and the crude extract incubated for 30 min on ice. The proteins were then extracted by ultrasonic treatments (6 × 30 s, 90 W) in ice and centrifugation (20,000 *g*, 15 min, 4°C). To purify recombinant SyLPD, PsmtLPD, AtTRXo1, and AtNTRa, we performed nickel-nitrilotriacetic acid agarose affinity chromatography according to the protocol of the supplier (HisTrap; GE Healthcare). The eluted proteins were checked regarding purity using SDS-PAGE and staining by Coomassie Brilliant Blue and subsequently used for enzyme measurements.

## Isolation of Mitochondria and mtLPD Activity Measurements

To obtain mtLPD for activity measurements, mitochondria were isolated from ~50 g pea leaves according to Keech et al. (2005). To perform enzyme activity measurements, mitochondria were solubilized by three freeze-thaw cycles, followed by 45-min centrifugation (40,000 *g*, 4°C). The obtained supernatant was used to determine the protein content. Total mtLPD activity in mitochondrial extracts or of recombinant proteins was assayed spectrophotometrically at 25°C as described previously (Timm et al., 2015). The reactions were initiated by adding 10–20 $\mu$g mL$^{-1}$ mitochondrial or 5–10 $\mu$g mL$^{-1}$ recombinant protein. Enzyme activity was determined without (control, oxidizing conditions) or after (reducing conditions) addition with 2 mM DTT for 10 min at room temperature. Furthermore, the artificial proton donor DTT was exchanged with a native mitochondrial redox-system consisting of TRXo1 and NTRa. Briefly, 30 $\mu$g NTRa and 12 $\mu$g TRXo1 were mixed with 100 $\mu$M NADPH in 100 $\mu$L potassium-phosphate, incubated for at least 10 min at 25°C; after addition of all other components of the test, mtLPD activity was monitored at 340 nm. For control measurements, the same reactions were carried out after boiling of TRXo1 and NTRa for 10 min at 90°C.

## Statistical Analysis

Significant values were determined using the two-tailed Student's *t* test (Microsoft Excel 10.0) and by ANOVA for multiple genotypes using the Holm and Sidak test for comparisons (Sigma Plot 11; Systat Software). The term significant is used here only if the change in question has been confirmed to be significant at the level of $^{*}P < 0.05$ or $^{**}P < 0.01$.

## Accession Numbers

The Arabidopsis Genome Initiative or GenBank/EMBL database contains sequence data from this article under the following accession numbers: TRXo1 (At2g35010), NTRa (At2g17420), GDC-T (At1g11680), GDC-P1 (At4g33010), GDC-H1 (At1g32470), GDC-L1 (mtLPD1; At1g48030), GDC-L2 (AT3G17240), SHMT1 (At4g37930), pMDH1 (At2g22780), HPR1 (At1g68010), PGLP1 (At5g35700), ODGC-E2 (At5g55070), PDC-E2 (At3g52200), RbcL (ATCG00490), 40S ribosomal protein S16 (At2g09990), pea LPD (P31023), maize LPD (A0A1D6MSE3), Syn LPD (P72740), *E. coli* LPD (P0A9P0), *Azotobacter vinelandii* LPD (C1DGW2), and *Pseudomonas putida* LPD (Q88C17).

## Supplemental Data

The following supplemental materials are available.

**Supplemental Figure S1.** Phenotype and PCR verification of the *TxGT* mutant.

**Supplemental Figure S2.** Expression of selected photorespiratory and TCA cycle enzymes during $CO_2$ transition.

**Supplemental Figure S3.** Alignment of LPD proteins from different sources.

**Supplemental Table S1.** Absolute metabolite contents in *trxo1* and the wild type during $CO_2$ transition.

**Supplemental Table S2.** Absolute metabolite contents in *trxo1*, *gldt1* and *TxGT* compared to the wild type grown in HC and LC conditions.

**Supplemental Table S3.** Oligonucleotides used during this study.

## ACKNOWLEDGMENTS

We thank Maria Wittmiß (Rostock) for introducing O.R. in enzymatic measurements and providing recombinant LPD of *Synechocystis* PCC6803 and the Nottingham Arabidopsis Stock Centre for the T-DNA insertional lines. We also acknowledge the technical assistance from Ina Krahnert (Potsdam-Golm). The donation of the *gldt1-1* mutant line and photorespiratory antibodies was received from Hermann Bauwe (University of Rostock, Germany) and the pMDH antibody from Steven M. Smith (University of Tasmania, Australia).

Received May 8, 2019; accepted July 30, 2019; published August 14, 2019.

## LITERATURE CITED

**Alonso JM, Stepanova AN, Leisse TJ, Kim CJ, Chen H, Shinn P, Stevenson DK, Zimmerman J, Barajas P, Cheuk R, et al** (2003) Genome-wide insertional mutagenesis of *Arabidopsis thaliana.* Science **301:** 653–657

**Anderson LE** (1971) Chloroplast and cytoplasmic enzymes. II. Pea leaf triose phosphate isomerases. Biochim Biophys Acta **235:** 237–244

**Appel AM, Bercaw JE, Bocarsly AB, Dobbek H, DuBois DL, Dupuis M, Ferry JG, Fujita E, Hille R, Kenis PJA, et al** (2013) Frontiers, opportunities, and challenges in biochemical and chemical catalysis of $CO_2$ fixation. Chem Rev **113:** 6621–6658

**Arrivault S, Guenther M, Ivakov A, Feil R, Vosloh D, van Dongen JT, Sulpice R, Stitt M** (2009) Use of reverse-phase liquid chromatography, linked to tandem mass spectrometry, to profile the Calvin cycle and other metabolic intermediates in Arabidopsis rosettes at different carbon dioxide concentrations. Plant J **59:** 826–839

**Arrivault S, Guenther M, Fry SC, Fuenfgeld MMFF, Veyel D, Mettler-Altmann T, Stitt M, Lunn JE** (2015) Synthesis and use of stable-isotope-labeled internal standards for quantification of phosphorylated metabolites by LC-MS/MS. Anal Chem **87:** 6896–6904

**Badger MR, Fallahi H, Kaines S, Takahashi S** (2009) Chlorophyll fluorescence screening of *Arabidopsis thaliana* for $CO_2$ sensitive photorespiration and photoinhibition mutants. Funct Plant Biol **36:** 867–873

**Balmer Y, Vensel WH, Tanaka CK, Hurkman WJ, Gelhaye E, Rouhier N, Jacquot JP, Manieri W, Schürmann P, Droux M, Buchanan BB** (2004) Thioredoxin links redox to the regulation of fundamental processes of plant mitochondria. Proc Natl Acad Sci USA **101:** 2642–2647

**Bauwe H, Hagemann M, Fernie AR** (2010) Photorespiration: Players, partners and origin. Trends Plant Sci **15:** 330–336

**Bauwe H, Hagemann M, Kern R, Timm S** (2012) Photorespiration has a dual origin and manifold links to central metabolism. Curr Opin Plant Biol **15:** 269–275

**Betti M, Bauwe H, Busch FA, Fernie AR, Keech O, Levey M, Ort DR, Parry MAJ, Sage R, Timm S, et al** (2016) Manipulating photorespiration to increase plant productivity: Recent advances and perspectives for crop improvement. J Exp Bot **67:** 2977–2988

**Blackwell RD, Murray AJS, Lea PJ, Kendall AC, Hall NP, Turner JC, Wallsgrove RM** (1988) The value of mutants unable to carry out photorespiration. Photosynth Res **16:** 155–176

**Bourguignon J, Neuburger M, Douce R** (1988) Resolution and characterization of the glycine-cleavage reaction in pea leaf mitochondria. Properties of the forward reaction catalysed by glycine decarboxylase and serine hydroxymethyltransferase. Biochem J **255:** 169–178

**Bowes G, Ogren WL, Hageman RH** (1971) Phosphoglycolate production catalyzed by ribulose diphosphate carboxylase. Biochem Biophys Res Commun **45:** 716–722

**Boyes DC, Zayed AM, Ascenzi R, McCaskill AJ, Hoffman NE, Davis KR, Görlach J** (2001) Growth stage-based phenotypic analysis of Arabidopsis:

A model for high throughput functional genomics in plants. Plant Cell **13:** 1499–1510

**Bradford MM** (1976) A rapid and sensitive method for the quantitation of microgram quantities of protein utilizing the principle of protein-dye binding. Anal Biochem **72:** 248–254

**Carroll AJ, Zhang P, Whitehead L, Kaines S, Tcherkez G, Badger MR** (2015) PhenoMeter: A metabolome database search tool using statistical similarity matching of metabolic phenotypes for high-confidence detection of functional links. Front Bioeng Biotechnol **3:** 106

**Cousins AB, Walker BJ, Pracharoenwattana I, Smith SM, Badger MR** (2011) Peroxisomal hydroxypyruvate reductase is not essential for photorespiration in Arabidopsis but its absence causes an increase in the stoichiometry of photorespiratory $CO_2$ release. Photosynth Res **108:** 91–100

**da Fonseca-Pereira P, Souza PVL, Hou LY, Schwab S, Geigenberger P, Nunes-Nesi A, Timm S, Fernie AR, Thormählen I, Araújo WL, Daloso DM** (2019) Thioredoxin *h2* contributes to the redox regulation of mitochondrial photorespiratory metabolism. Plant Cell Environ doi:10.1111/pce.13640

**Daloso DM, Müller K, Obata T, Florian A, Tohge T, Bottcher A, Riondet C, Bariat L, Carrari F, Nunes-Nesi A, et al** (2015) Thioredoxin, a master regulator of the tricarboxylic acid cycle in plant mitochondria. Proc Natl Acad Sci USA **112:** E1392–E1400

**Dellero Y, Lamothe-Sibold M, Jossier M, Hodges M** (2015) *Arabidopsis thaliana* ggt1 photorespiratory mutants maintain leaf carbon/nitrogen balance by reducing RuBisCO content and plant growth. Plant J **83:** 1005–1018

**Douce R, Bourguignon J, Neuburger M, Rébeillé F** (2001) The glycine decarboxylase system: A fascinating complex. Trends Plant Sci **6:** 167–176

**Eisenhut M, Ruth W, Haimovich M, Bauwe H, Kaplan A, Hagemann M** (2008) The photorespiratory glycolate metabolism is essential for cyanobacteria and might have been conveyed endosymbiontically to plants. Proc Natl Acad Sci USA **105:** 17199–17204

**Eisenhut M, Planchais S, Cabassa C, Guivarc'h A, Justin AM, Taconnat L, Renou JP, Linka M, Gagneul D, Timm S, et al** (2013) Arabidopsis A BOUT DE SOUFFLE is a putative mitochondrial transporter involved in photorespiratory metabolism and is required for meristem growth at ambient $CO_2$ levels. Plant J **73:** 836–849

**Eisenhut M, Bräutigam A, Timm S, Florian A, Tohge T, Fernie AR, Bauwe H, Weber A** (2017) Photorespiration is crucial to the dynamic response of photosynthetic metabolism to altered $CO_2$ availability. Mol Plant **10:** 47–61

**Faure M, Bourguignon J, Neuburger M, MacHerel D, Sieker L, Ober R, Kahn R, Cohen-Addad C, Douce R** (2000) Interaction between the lipoamide-containing H-protein and the lipoamide dehydrogenase (L-protein) of the glycine decarboxylase multienzyme system 2. Crystal structures of H- and L-proteins. Eur J Biochem **267:** 2890–2898

**Fernie AR, Bauwe H, Eisenhut M, Florian A, Hanson DT, Hagemann M, Keech O, Mielewczik M, Nikoloski Z, Peterhänsel C, et al** (2013) Perspectives on plant photorespiratory metabolism. Plant Biol (Stuttg) **15:** 748–753

**Flügel F, Timm S, Arrivault S, Florian A, Stitt M, Fernie AR, Bauwe H** (2017) The photorespiratory metabolite 2-phosphoglycolate regulates photosynthesis and starch accumulation in Arabidopsis. Plant Cell **29:** 2537–2551

**Foyer CH, Bloom AJ, Queval G, Noctor G** (2009) Photorespiratory metabolism: Genes, mutants, energetics, and redox signaling. Annu Rev Plant Biol **60:** 455–484

**Geigenberger P, Thormählen I, Daloso DM, Fernie AR** (2017) The unprecedented versatility of the plant thioredoxin system. Trends Plant Sci **22:** 249–262

**Hasse D, Andersson E, Carlsson G, Masloboy A, Hagemann M, Bauwe H, Andersson I** (2013) Structure of the homodimeric glycine decarboxylase P-protein from Synechocystis sp. PCC 6803 suggests a mechanism for redox regulation. J Biol Chem **288:** 35333–35345

**Hodges M, Jossier M, Boex-Fontvieille E, Tcherkez G** (2013) Protein phosphorylation and photorespiration. Plant Biol (Stuttg) **15:** 694–706

**Hodges M, Dellero Y, Keech O, Betti M, Raghavendra AS, Sage R, Zhu XG, Allen DK, Weber AP** (2016) Perspectives for a better understanding of the metabolic integration of photorespiration within a complex plant primary metabolism network. J Exp Bot **67:** 3015–3026

**Hoffmann C, Plocharski B, Haferkamp I, Leroch M, Ewald R, Bauwe H, Riemer J, Herrmann J, Neuhaus E** (2013) From endoplasmic reticulum to mitochondria: Absence of the Arabidopsis ATP antiporter ER-ANT1 perturbs photorespiration. Plant Cell **25:** 2647–2660

**Keech O, Dizengremel P, Gardeström P** (2005) Preparation of leaf mitochondria from *Arabidopsis thaliana*. Physiol Plant **124:** 403–409

**Keech O, Gardeström P, Kleczkowski LA, Rouhier N** (2017) The redox control of photorespiration: From biochemical and physiological aspects to biotechnological considerations. Plant Cell Environ **40:** 553–569

**Kelly GJ, Latzko E** (1976) Inhibition of spinach-leaf phosphofructokinase by 2-phosphoglycollate. FEBS Lett **68:** 55–58

**Laloi C, Rayapuram N, Chartier Y, Grienenberger JM, Bonnard G, Meyer Y** (2001) Identification and characterization of a mitochondrial thioredoxin system in plants. Proc Natl Acad Sci USA **98:** 14144–14149

**Leegood RC, Lea PJ, Adcock MD, Häusler RE** (1995) The regulation and control of photorespiration. J Exp Bot **46:** 1397–1414

**Levey M, Timm S, Mettler-Altmann T, Luca Borghi G, Koczor M, Arrivault S, Pm Weber A, Bauwe H, Gowik U, Westhoff P** (2019) Efficient 2-phosphoglycolate degradation is required to maintain carbon assimilation and allocation in the $C_4$ plant *Flaveria bidentis*. J Exp Bot **70:** 575–587

**Li J, Weraduwage SM, Preiser AL, Tietz S, Weise SE, Strand DD, Froehlich JE, Kramer DM, Hu J, Sharkey TD** (2019) A cytosolic bypass and G6P shunt in plants lacking peroxisomal hydroxypyruvate reductase. Plant Physiol **180:** 783–792

**López-Calcagno PE, Fisk S, Brown KL, Bull SE, South PF, Raines CA** (2018) Overexpressing the H-protein of the glycine cleavage system increases biomass yield in glasshouse and field-grown transgenic tobacco plants. Plant Biotechnol J **17:** 141–151

**Millar AH, Knorpp C, Leaver CJ, Hill SA** (1998) Plant mitochondrial pyruvate dehydrogenase complex: Purification and identification of catalytic components in potato. Biochem J **334:** 571–576

**Nakamura Y, Kanakagiri S, Van K, He W, Spalding MH** (2005) Disruption of the glycolate dehydrogenase gene in the high-$CO_2$-requiring mutant HCR89 of Chlamydomonas reinhardtii. Can J Bot **83:** 820–833

**Obata T, Florian A, Timm S, Bauwe H, Fernie AR** (2016) On the metabolic interactions of (photo)respiration. J Exp Bot **67:** 3003–3014

**Ogren WL, Bowes G** (1971) Ribulose diphosphate carboxylase regulates soybean photorespiration. Nat New Biol **230:** 159–160

**Oliver DJ, Sarojini G** (1987) Regulation of glycine decarboxylase by serine. *In* Progress in photosynthesis research, J Biggins, ed. **Vol III**. Martinus Nijhoff, Dordrecht, pp 573–576

**Oliver DJ, Neuburger M, Bourguignon J, Douce R** (1990) Interaction between the component enzymes of the glycine decarboxylase multienzyme complex. Plant Physiol **94:** 833–839

**Orf I, Timm S, Bauwe H, Fernie AR, Hagemann M, Kopka J, Nikoloski Z** (2016) Can cyanobacteria serve as a model of plant photorespiration? - a comparative meta-analysis of metabolite profiles. J Exp Bot **67:** 2941–2952

**Palmieri MC, Lindermayr C, Bauwe H, Steinhauser C, Durner J** (2010) Regulation of plant glycine decarboxylase by *s*-nitrosylation and glutathionylation. Plant Physiol **152:** 1514–1528

**Pérez-Pérez ME, Mauriès A, Maes A, Tourasse NJ, Hamon M, Lemaire SD, Marchand CH** (2017) The deep thioredoxome in *Chlamydomonas reinhardtii*: New insights into redox regulation. Mol Plant **10:** 1107–1125

**Peterhänsel C, Krause K, Braun H-P, Espie GS, Fernie AR, Hanson DT, Keech O, Maurino VG, Mielewczik M, Sage RF** (2013) Engineering photorespiration: Current state and future possibilities. Plant Biol (Stuttg) **15:** 754–758

**Pick TR, Bräutigam A, Schulz MA, Obata T, Fernie AR, Weber APM** (2013) PLGG1, a plastidic glycolate glycerate transporter, is required for photorespiration and defines a unique class of metabolite transporters. Proc Natl Acad Sci USA **110:** 3185–3190

**Pracharoenwattana I, Cornah JE, Smith SM** (2007) Arabidopsis peroxisomal malate dehydrogenase functions in $\beta$-oxidation but not in the glyoxylate cycle. Plant J **50:** 381–390

**Queval G, Noctor G** (2007) A plate reader method for the measurement of NAD, NADP, glutathione, and ascorbate in tissue extracts: Application to redox profiling during Arabidopsis rosette development. Anal Biochem **363:** 58–69

**Rademacher N, Kern R, Fujiwara T, Mettler-Altmann T, Miyagishima SY, Hagemann M, Eisenhut M, Weber AP** (2016) Photorespiratory glycolate

oxidase is essential for the survival of the red alga Cyanidioschyzon merolae under ambient $CO_2$ conditions. J Exp Bot **67:** 3165–3175

**Reichheld JP, Meyer E, Khafif M, Bonnard G, Meyer Y** (2005) AtNTRB is the major mitochondrial thioredoxin reductase in *Arabidopsis thaliana*. FEBS Lett **579:** 337–342

**Reumann S, Weber APM** (2006) Plant peroxisomes respire in the light: Some gaps of the photorespiratory C2 cycle have become filled--others remain. Biochim Biophys Acta **1763:** 1496–1510

**Simkin A, Lopez-Calcagno P, Davey P, Headland L, Lawson T, Timm S, Bauwe H, Raines C** (2017) Simultaneous stimulation of the edoheptulose 1,7-bisphosphatase, fructose 1,6-bisphophate aldolase and the photorespiratory glycine decarboxylase-H protein increases $CO_2$ assimilation, vegetative biomass and seed yield in Arabidopsis. Plant Biotechnol J **15:** 805–816

**Somerville CR** (2001) An early Arabidopsis demonstration. Resolving a few issues concerning photorespiration. Plant Physiol **125:** 20–24

**Somerville CR, Ogren WL** (1979) Phosphoglycolate phosphatase-deficient mutant of Arabidopsis. Nature **280:** 833–836

**South PF, Cavanagh AP, Lopez-Calcagno PE, Raines CA, Ort DR** (2018) Optimizing photorespiration for improved crop productivity. J Integr Plant Biol **60:** 1217–1230

**South PF, Cavanagh AP, Liu HW, Ort DR** (2019) Synthetic glycolate metabolism pathways stimulate crop growth and productivity in the field. Science **363:** eaat9077

**Suzuki K, Marek LF, Spalding MH** (1990) A photorespiratory mutant of *Chlamydomonas reinhardtii*. Plant Physiol **93:** 231–237

**Timm S, Bauwe H** (2013) The variety of photorespiratory phenotypes - employing the current status for future research directions on photorespiration. Plant Biol (Stuttg) **15:** 737–747

**Timm S, Florian A, Jahnke K, Nunes-Nesi A, Fernie AR, Bauwe H** (2011) The hydroxypyruvate-reducing system in Arabidopsis: Multiple enzymes for the same end. Plant Physiol **155:** 694–705

**Timm S, Florian A, Arrivault S, Stitt M, Fernie AR, Bauwe H** (2012a) Glycine decarboxylase controls photosynthesis and plant growth. FEBS Lett **586:** 3692–3697

**Timm S, Mielewczik M, Florian A, Frankenbach S, Dreissen A, Hocken N, Fernie AR, Walter A, Bauwe H** (2012b) High-to-low $CO_2$ acclimation reveals plasticity of the photorespiratory pathway and indicates regulatory links to cellular metabolism of Arabidopsis. PLoS One **7:** e42809

**Timm S, Florian A, Wittmiß M, Jahnke K, Hagemann M, Fernie AR, Bauwe H** (2013) Serine acts as a metabolic signal for the transcriptional control of photorespiration-related genes in Arabidopsis. Plant Physiol **162:** 379–389

**Timm S, Wittmiß M, Gamlien S, Ewald R, Florian A, Frank M, Wirtz M, Hell R, Fernie AR, Bauwe H** (2015) Mitochondrial dihydrolipoyl dehydrogenase activity shapes photosynthesis and photorespiration of *Arabidopsis thaliana*. Plant Cell **27:** 1968–1984

**Timm S, Florian A, Fernie AR, Bauwe H** (2016) The regulatory interplay between photorespiration and photosynthesis. J Exp Bot **67:** 2923–2929

**Timm S, Giese J, Engel N, Wittmiß M, Florian A, Fernie AR, Bauwe H** (2018) T-protein is present in large excess over the other proteins of the glycine cleavage system in leaves of Arabidopsis. Planta **247:** 41–51

**Tolbert NE** (1971) Microbodies peroxisomes and glyoxysomes. Annu Rev Plant Physiol **22:** 45–74

**Vauclare P, Diallo N, Bourguignon J, Macherel D, Douce R** (1996) Regulation of the expression of the glycine decarboxylase complex during pea leaf development. Plant Physiol **112:** 1523–1530

**Walker JL, Oliver DJ** (1986) Light-induced increases in the glycine decarboxylase multienzyme complex from pea leaf mitochondria. Arch Biochem Biophys **248:** 626–638

**Walker BJ, VanLoocke A, Bernacchi CJ, Ort DR** (2016) The costs of photorespiration to food production now and in the future. Annu Rev Plant Biol **67:** 107–129

**Wingler A, Lea PJ, Quick WP, Leegood RC** (2000) Photorespiration: Metabolic pathways and their role in stress protection. Philos Trans R Soc Lond B Biol Sci **355:** 1517–1529

**Woody ST, Austin-Phillips S, Amasino RM, Krysan PJ** (2007) The *WiscDsLox* T-DNA collection: An Arabidopsis community resource generated by using an improved high-throughput T-DNA sequencing pipeline. J Plant Res **120:** 157–165

**Zelitch I** (1964) Organic acids and respiration in photosynthetic tissues. Annu Rev Plant Physiol **15:** 121–142

**Zelitch I, Schultes NP, Peterson RB, Brown P, Brutnell TP** (2009) High glycolate oxidase activity is required for survival of maize in normal air. Plant Physiol **149:** 195–204

**Zhang X, Zheng X, Ke S, Zhu H, Liu F, Zhang Z, Peng X, Guo L, Zeng R, Hou P, et al** (2016) ER-localized adenine nucleotide transporter ER-ANT1: An integrator of energy and stress signaling in rice. Plant Mol Biol **92:** 701–715